Determination of spectral sensitivity of a vacuum ultraviolet, grazing incidence spectrograph

by

Hana Ohkawa
B.S., Physics (1994)
Massachusetts Institute of Technology

Submitted to the Department of Physics
and the Department of Electrical Engineering and Computer Science
in partial fulfillment of the requirements for the degrees of
Master of Science in Physics
and
Master of Science in Electrical Engineering
at the
MASSACHUSETTS INSTITUTE OF TECHNOLOGY
June 1997

Author .....
Department of Physics
May 23, 1997

Certified by .....
James L. Terry, Research Scientist, PSFC
Thesis Supervisor

Certified by .....
Miklos Porkolab, Professor of Physics
Thesis Supervisor

Accepted by .....
George Koster, Professor of Physics
Chairman, Departmental Committee on Graduate Students

Accepted by .....
Arthur C. Smith, Professor of Electrical Engineering
Chairman, Departmental Committee on Graduate Theses

Determination of spectral sensitivity of a vacuum ultraviolet, grazing incidence spectrograph

by

Hana Ohkawa

Submitted to the Department of Physics
and the Department of Electrical Engineering and Computer Science
on May 23, 1997, in partial fulfillment of the
requirements for the degrees of
Master of Science in Physics
and
Master of Science in Electrical Engineering

Abstract

The spectral sensitivity of the vacuum ultraviolet (VUV) grazing incidence spectrometer on Alcator C-Mod is calibrated in the spectral region from 200 Å through 1100 Å using the branching ratio method. This technique uses the known branching ratio between visible and ultraviolet lines which share the same upper state, and requires simultaneous measurement of emission in the VUV and in the visible along the same line of sight. Electron cyclotron discharge cleaning (ECDC) and fusion plasmas in C-Mod were used as the calibration sources. Three line pairs from the ions D I and He II were successfully used, supplying the absolute sensitivity of the VUV spectrograph at three wavelengths: 243 Å, 972 Å, and 1025 Å. A line pair from He I was found unsuitable for this technique, because of self-absorption of the VUV line.

Thesis Supervisor: James L. Terry, Research Scientist, PSFC

Thesis Supervisor: Miklos Porkolab, Professor of Physics

Acknowledgments

The author would like to thank James Terry for three years of first class supervision, and the many weekend and late hours spent gathering data for this thesis.

Thanks also to:

- Miklos Porkolab for reading this thesis, general guidance, and keeping C-Mod alive through the budget crisis,
- John Rice, John Goetz, and Bruce Lipschultz, for answering my questions and other scientist stuff,
- Aaron Allen, Jim Weaver, Dimitrios Pappas, and Dirk Lumma, for making the workplace fun,
- Rob Nachtrieb for answering all my sundry questions with aplomb and unerring accuracy,
- Bruno Coppi for his guidance, and all his work in fusion,
- My family and friends for their support and love

A special thanks to Frank Silva for all of his help and for his general dedication to C-Mod.

Contents

List of Figures

Chapter 1

Thesis Goals and Outline

For this thesis, the branching ratio method was used to calibrate the VUV grazing incidence spectrometer of Alcator C-Mod, a tokamak fusion device operating at the Plasma Fusion and Science Center of the Massachussetts Institute of Technology.

The VUV spectrometer had been previously calibrated with other methods, but it was believed that the sensitivity of the instrument had degraded. A new technique was needed, which would allow frequent checks of the calibration. The branching ratio method was selected because it can be done in situ, and because it is relatively simple.

The method employs the known branching ratio between dipole lines which share the same upper state. Pairs are chosen with one line in the spectral range of the VUV spectrograph, and the other in the range of an absolutely calibrated visible instrument. When the two instruments view the same source, the brightnesses are related by the branching ratios. Then, the sensitivity of the VUV spectrograph can be determined from the sensitivity of the visible instrument, at a single wavelength for each pair. If enough pairs are used, intermediate wavelengths can be interpolated.

A system for measuring visible emission was designed and built specifically for the purpose of this calibration. The tokamak fusion plasma and electron discharge cleaning plasma were used as the calibration sources.

1.1 Motivations

A reliable absolute calibration of the VUV spectrograph is essential for several important ongoing studies at C-Mod. The absolute calibration of the VUV spectrograph was planned when it became clear that the old calibration was inaccurate. Comparisons of VUV data with another spectrograph showed that the sensitivity had degraded by approximately a factor of three at 75 Å.

Since the brightness of a line depends on so many factors, the brightnesses measured by the VUV spectrograph by themselves can only be used to determine relative impurity concentrations. When combined with the data of other plasma diagnostics, analysis of the absolute brightnesses yields even more information.

Most commonly, the VUV data have been used with a 1-D transport model to find the total density of various impurities. The model, called the Multi Impurity Species Transport (MIST) code, uses measured electron temperature and density profiles, calculated rate coefficients, and empirical transport coefficients to determine the spatial profiles of the various charge states of an impurity.

The MIST code assumes an arbitrary total impurity density. The brightness of a line from a given charge state is calculated by line integrating the product of the excitation rate coefficient, the electron density, and the density of the charge state along the line of sight. This brightness is compared with that measured by the VUV spectrograph. The ratio of the brightnesses equals the ratio of the true impurity density to the density assumed by MIST.

As an initial part of this work, the MIST code has been implemented and run for many impurities, including boron, carbon, nitrogen, oxygen, fluorine, neon, and molybdenum. The impurity densities unfolded from the line brightness data have been used in studies of impurity screening. The low recycling gaseous impurities, nitrogen and methane were puffed into the plasma, and the core density was found to be proportional to the rate of injection [1]. The total impurity density was also used to compare screening in detached and attached plasmas. While the absolute

calibration is not needed to study the relative time evolution of the core density, it is essential for determining the proportionality constant between the core density and injection rate.

The absolute calibration is also important when the VUV data is combined with that of another spectrograph. Studies of molybdenum transport have used the brightness profiles of VUV and x-ray lines to refine the atomic physics rates used in the MIST transport code [2]. The atomic physics rate coefficients previously used were shown to be inaccurate, and new theoretical rates were calculated. These new rate coefficients included direct collisional ionization, excitation-autoionization, and dielectronic and radiative recombination [2]. Predictions based on the new rates provided a good match to the measured profiles of the various molybdenum ionization states. For this study, the x-ray data measured by C-Mod's high resolution x-ray spectrograph (HIREX) were combined with the VUV spectrograph data. A dependable absolute calibration of the VUV spectrograph is critical for such comparisons with other spectrometers.

1.2 Outline

- Chapter 2 provides background information for those unfamiliar with fusion, tokamaks, or VUV spectroscopy.
- Chapter 3 discusses the branching ratio method in detail, weighs the advantages and disadvantages, and presents the lines which were used in the calibration.
- Chapter 4 describes the Alcator C-Mod tokamak and the VUV grazing incidence spectrometer.
- Chapter 5 covers the design and calibration of the Visible System.
- Chapter 6 details the results of the calibration measurements, and makes recommendations for future work.

Chapter 2

Background

2.1 Fusion

As an alternative energy source, nuclear fusion has many attractive characteristics. The fuel, deuterium, is present in ordinary sea water. The reaction is clean and cannot runaway in the fashion of nuclear fission. Consequently, it has long been an ambition of scientists to create a fusion power plant. The first man-made fusion device was the hydrogen bomb detonated at Eniwetok Atoll, in 1952. The early fusion researchers who designed the bomb predicted that the fusion problem could be solved with a decade or two.

Almost fifty years later, many experimental devices have been built to study the problem, but none could function as power plants. These devices operate with large energy deficits, requiring tremendous amounts of energy to create fusion reactions. The fusion problem has proved to be complex and subtle.

Fusion occurs when two light atomic nuclei combine to form a single more massive nucleus, with a smaller fragment or particle carrying the requisite momentum from the collision. The reactions usually considered the most promising for commercial reactors are:

$$D + D \rightarrow^3 He + n + 3.2MeV, \tag{2.1}$$

$$D + D \rightarrow T + p + 4.0MeV, \tag{2.2}$$

$$D + T \rightarrow^4 He + n + 17.6MeV, \tag{2.3}$$

where D and T are the isotopes of hydrogen, deuterium and tritium. Though these reactions are energetically favorable, they occur only at extreme temperatures. The nuclear strong force which binds the nuclei is highly localized, so the two nuclei must be very close for fusion to occur. At conventional temperatures, the Coulomb repulsion of the two positively charged nuclei prevents the nuclei from coming close enough to combine. Colliding accelerating beams of nuclei with targets does not result in a significant rate of fusion reactions, because most of the nuclei lose their energy by scattering before fusion can occur. A thermal distribution of high energy nuclei is needed. For the D-T reaction of equation (2.3), the Coulomb repulsion can be overcome at temperatures on the order of 10 million degrees Celsius.

2.2 Plasmas

At temperatures far smaller than those required for fusion, matter becomes a plasma. A plasma is commonly defined as a gas which is partially or completely ionized, and exhibits collective behavior [3]. Under certain conditions, gases can become plasmas. In a fusion reactor, the high temperature of the particles results in high speed collisions which strip the nuclei of their bound electrons, creating a plasma of positively and negatively charged particles.

2.3 Confinement

The confinement of high temperature plasmas is a difficult problem. One approach is to start with a cold fuel pellet and heat it so quickly, the inertia of the pellet keeps it together long enough for the fusions to occur. For the NOVA 'inertial confinement' device, high power lasers deliver 200 kJ of energy to the fuel pellet in less than a nanosecond [4].

Magnetic confinement of plasmas is the most popular approach. Charged particles interact strongly with electric and magnetic fields. These fields are a powerful tool for confining and controlling plasma flows, if the fields can be generated in a favorable configuration. A plasma can be suspended in a vacuum with a minimum of material contact. Magnetic geometries can be devised which predict near perfect confinement for simplistic single particle models. However, the behavior of plasmas is extremely complex and difficult to predict, with many collective and statistical effects.

The most successful magnetic geometry has been the toroidal field shape used in machines dubbed tokamaks, from the Russian acronym for 'toroidal magnetic chamber.' Toroidal coordinates are illustrated in Figure 2-1. The plasma is guided by a powerful toroidal magnetic field, generated by large coils which wrap around the vacuum vessel. However, particles tend to drift perpendicular to the field when following the curving toroidal field line. The presence of a poloidal field component improves confinement. In a tokamak, this poloidal field is generated by the plasma itself, when a significant toroidal current is driven through the plasma, which is an excellent conductor. For a hydrogen plasma with an electron temperature of 2500 eV, the resistivity is approximately 25% that of copper. The plasma current is typically driven by induction, though alternate methods have been explored.

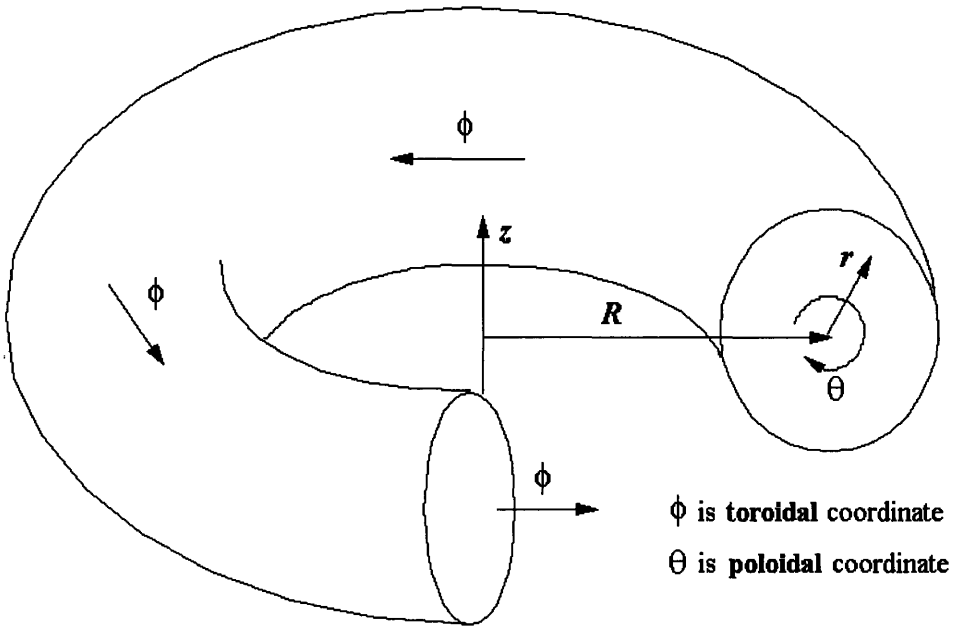

Figure 2-1: Toroidal coordinates The coordinates associated with the toroidal geometry are shown. R is called the major radius, and r is the minor radius. The coordinate z is commonly used especially when working with cross-sections, as in Figure 5-1.

2.4 Vacuum Ultra-Violet Spectroscopy on Tokamaks

The study of fusion plasmas has spurred the development of advanced plasma diagnostics. Because of the high temperature and vacuum conditions inside the machine vessel, it is rarely possible to make direct measurements of plasma characteristics. Important parameters such as density and temperature must be inferred from radiation patterns, particle emissions, and magnetics measurements. A typical tokamak has dozens of distinct diagnostics in operation.

At the high temperatures of fusion plasmas, many of the important line emissions occur in the vacuum ultraviolet (VUV) and x-ray portion of the electromagnetic spectrum, from impurities always present in a real laboratory plasma. It is notoriously difficult to make measurements in the VUV, because these photons are so readily absorbed by almost any material. In fact, VUV radiation is absorbed by the oxygen in air. Consequently, for measurements in this spectral region, the path from source to detector must be under vacuum.

The plasma chamber of a tokamak is a vacuum vessel designed for the relatively low particle densities needed to create a fusion plasma. Ion species which are not part of the desired fusion reaction are called impurities. While useful for diagnostic information, impurities are, in general, highly undesirable in the plasma core, because they tend to cool the plasma. Special techniques for treating the inside of the vacuum vessel have been developed for eliminating impurities, including oxygen.

Since the vessel contains a minimal amount of oxygen, there is good transmission of VUV radiation to the measurement ports. For other tokamak diagnostics using x-ray, visible, UV, or IR emissions, the plasma can be viewed through sapphire, quartz, (UV through IR) or thin beryllium (x-rays) windowed ports. For a VUV diagnostic, the detector must share the vacuum with the plasma, since VUV cannot penetrate material windows.

The VUV is considered to extend from about 10 to 2000 Å[5]. The upper limit is defined by the end of the continuous absorption of oxygen. The lower limit is where the VUV meets the soft x-ray spectrum. The energies of VUV photons are on the order of 100 eV, which is why the hot fusion plasma emits strongly in this region. Any potential calibration source would have to operate at similar temperatures or beam energy. Platinum hollow cathode discharge lamps can be used for several lines above 1000 Å. Manson x-ray sources, which generate K_α lines of various anodes, provide illumination in the near x-ray region. While sources exist which can be used for the the rest of the VUV spectrum, they are not readily available. For example, synchrotrons provide a continuous spectrum across the VUV range, but are prohibitively expensive. It would also be too difficult to transport the VUV spectrograph to an existing synchrotron.

For this thesis, the branching ratio technique was used to calibrate C-Mod's VUV spectrograph. This method is explained in detail in Chapter 3. The tokamak electron cyclotron discharge cleaning (ECDC) and fusion plasmas were used as the calibration sources. ECDC plasmas are described in detail in Section 6.1.

The brightness of the plasma is generally unknown, so simultaneous measurements must be made with the uncalibrated VUV spectrometer and with a calibrated visible detector. Dipole lines which share the same upper state are emitted in a ratio which can be calculated from knowledge of the atomic physics. Pairs of transitions have been selected which have one line in the visible and one in the VUV region.

Chapter 3

The Branching Ratio Method

The branching ratio method is in principle, one of the simplest techniques for calibration in the VUV region. This chapter reviews the principles of the technique, advantages, disadvantages, and presents the lines which were used in this thesis.

3.1 Theory

The idea behind the branching ratio method is simple. Pairs of lines are selected which meet these criteria:

- The lines share the same upper state
- The transition probabilities for both lines are accurately known from atomic physics calculations
- One line is in the spectral range of an absolutely calibrated (reference) spectrometer
- The other line is in the spectral range of the instrument which is to be calibrated

For use of the branching ratio method, the two instruments must view the same or a similar source. Typically, an instrument which measures visible light is chosen

as the reference spectrograph. Absolutely calibrated sources are readily available in this spectral region, and a dependable calibration can be accomplished with relative ease. The two spectrometers must be positioned so that they can make simultaneous measurements of the source. The measurement by the reference spectrometer determines the brightness of the visible line in the viewed region. The brightness of the VUV line can be calculated from the transition probabilities. The comparison of this brightness and the value measured by the VUV spectrometer gives the sensitivity at this wavelength. If many pairs are used, the sensitivity at intermediate wavelengths can be interpolated with reasonable accuracy.

The calculation of the relative intensities follows from the application of the general equation for the radiative intensity I(power/volume) of an optically thin emission line. For transition from an atomic state k to a lower state i, the intensity is given by [6]

$$I_{ki} = N_k A_{ki} h\nu_{ik}, \tag{3.1}$$

where N_k is the number density of atoms or ions populating the state k, A_{ki} is the probability of transition from state k to i by spontaneous emission, with units of frequency, h is Planck's constant, and ν_{ik} is the frequency of the emitted photon. The product $h\nu_{ik}$ is the energy of the emitted photons. Further, since the medium between plasma emission and detectors is essentially non-dispersive,

$$h\nu = \frac{hc}{\lambda}. \tag{3.2}$$

Then the intensity of the VUV line can be calculated from the visible line intensity according to

$$I_{VUV} = \frac{A_{VUV}\lambda_{visible}}{A_{visible}\lambda_{VUV}} I_{visible}. \tag{3.3}$$

The quantity measured by spectrometers viewing a source is brightness, also known as surface brightness, B(power/unit solid angle/area), related to the intensity by

$$B \equiv \frac{\int I(l)dl}{4\pi}, \tag{3.4}$$

where the line integral is performed along the line of sight of the instrument. The ratio of the brightnesses of two lines is the same as the ratio of the intensities, i.e.

$$B_{VUV} = \frac{A_{VUV}\lambda_{visible}}{A_{visible}\lambda_{VUV}} B_{visible}. \tag{3.5}$$

3.2 Advantages

A principal advantage of the branching ratio method is that the brightness of the source is measured in situ and is available as long as both instruments are operational. Because of the relatively high energy of the photons, the available VUV sources are limited in wavelength coverage, and may be difficult to implement, as discussed in Section 2.4. The fusion plasma is conveniently available to the fusion spectroscopist as a source, but the brightness of the various spectral components is not well known (and is what the spectroscopist ultimately wants to measure). The branching ratio method allows the use of the experimental plasma as the calibration source. The ECDC plasma, can also be used as a source, as was done in this thesis.

Using the plasma as a source has many advantages. The calibration conditions are nearly identical to the experimental conditions. The calibration can be checked during normal experimental run periods, without any change of configuration. Further, the experimental plasma is a rich source of radiation, with good coverage of the calibration region. Additional line pairs can be obtained by introduction of impurities through laser ablation or gas puffing [7].

Another important advantage is that the branching ratio technique bases the cal-

ibration on measurements in the visible portion of the spectrum. Extremely sensitive detectors and well calibrated "external" sources are available in the visible region.

3.3 Disadvantages and difficulties

The two most difficult tasks in implementing the branching ratio method are

- Configuring the experimental situation so that both instrument view the same region of the source
- Finding enough line pairs which meet the requirements

If only a few pairs are used, interpolated values for intermediate wavelengths become unreliable. A handful of line pairs can be found which are native to a fusion plasma. Researchers have supplemented these by introducing impurities for additional line pairs. Relative calibration can also be done with pairs with both lines in the VUV. These results can be combined with absolute calibrations for a more complete spectral sensitivity curve.

The number of eligible candidates may be further diminished by contamination by other lines, or inadequate sensitivity. Various physical effects can cause the relative brightness to differ from the ratio predicted by equation (3.5). The most important are self-absorption in the lines, and quenching which has been observed in high density plasmas [6].

Self-absorption refers to light which is reabsorbed before reaching the instrument. If the density of the plasma is increased, the intensity of the detected light may initially increase, as the electron density and the density of the emitting ions grow. However, if the line integral of absorber density along the line of sight increases, self-absorption also increases. If the emitter/absorber density is further increased, the detected intensity may actually decrease. At very high density, the intensity will asymptote to the black body intensity for the electron temperature of the source, if it is in thermal equilibrium [8]. Significant self-absorption rarely occurs for visible and

VUV lines from magnetic fusion plasmas, and then only for ground state transitions of neutral atoms. Typically, the line density of possible absorbers must be greater than 10^{12} cm^{-2}.

Quenching is a general term for processes which result in a reduced intensity for a given line from the expected value. Quenching has been linked to the presence of magnetic fields, high pressure, chemical reactions, [9], [10], and other physical effects.

3.4 The Chosen Line Pairs

For this thesis work, the sources were hydrogen and helium ECDC. The line pairs are given in Table 3.1.

Ion	λ_{VUV} (Å)	Transition VUV	λ_{vis} (Å)	Transition visible	A_{VUV} (10^8 s^{-1})	A_{vis} (10^8 s^{-1}	$\frac{I_{VUV}}{I_{vis}}$
D I	972.27	1s-4p	4860.03	2s-4p	0.1278	0.08419	7.588
	1025.4	1s-3p	6561.03	2s-3p	0.5575	0.4410	8.088
He I	537.03	$1s^{21}S$ - $3p^1P^0$	5015.7	2s ^1S - $3p^1P^0$	5.73	0.141	380
He II	243.03	1s-4p	4685.7	3s-4p	2.045	1.438	27.42

Table 3.1: Branching ratio data for calibration lines The accuracy of the ratios is estimated to be 0.1%, for the lines of D I and He II, and 6% for the lines of He I.

Chapter 4

Alcator C-Mod and the VUV spectrometer

This chapter describes the experimental apparati which existed before this thesis work. The equipment designed for this thesis will be described in Chapter 5.

4.1 Alcator C-Mod

Alcator C-Mod is a tokamak fusion device operated at the Massachussetts Institute of Technology Plasma Fusion and Science Center. The original Alcator was the brain child of theoretical physicist Bruno Coppi, who postulated that a compact, high magnetic field, high density tokamak could achieve better confinement than previous geometries.

To achieve the high field and density, the Alcator C was designed with a low aspect ratio. The aspect ratio is the ratio of the major and minor radii, defined in Figure 2-1. A low aspect ratio corresponds to a 'bagel' like torus, while a high aspect ratio corresponds to a 'hula hoop' like torus. The 'bagel' shape of Alcator has several scientific advantages over the 'hula hoop.' However, the 'bagel' is difficult from an engineering standpoint, because there is precious little room through the center for

Parameter	Symbol	Typical	Maximum
Major Radius	R	0.67 m	-
Minor Radius	a	0.22 m	-
Elongation	κ	1.7	1.85
Toroidal Field	B_T	5.3 tesla	7.9 tesla
Density	n_e	1.5×10^{20} m^{-3}	1.2×10^{21} m^{-3}
Plasma Current	I_p	0.8 MA	1.5 MA
ICRF Power	P_{ICRF}	2 MW	3.5 MW

Table 4.1: Alcator C-Mod Parameters This table is reproduced from [11]. Elongation is a parameter which measures the non-circularity of the plasma. The ICRF power refers to the output power of the ion cyclotron radio frequency (ICRF) antennas which heat the plasma.

the passage of field coils and ohmic transformer.

C-Mod retains the 'bagel' shape of Alcator C but has advanced capacity for shaping the plasma, and controlling the plasma flow to material surfaces. Important parameters of the tokamak are summarized in Table 4.1. A cross sectional drawing of the C-Mod is Figure 4-1.

4.2 The VUV grazing incidence spectrometer

C-Mod's VUV time resolving spectrograph has operated in its present configuration for several years. The spectral resolution depends on which grating is used. For this thesis, a 300 line per mm grating was used, with a measured resolution of approximately

$$\frac{\lambda}{\Delta\lambda_{inst}} \sim 50 \text{ @ } 200 \text{ } \mathring{A}, 400 \text{ @ } 1000 \text{ } \mathring{A}. \tag{4.1}$$

The key elements of the VUV spectrograph are a gold grating, used in grazing incidence (88 degrees), a microchannel plate image intensifier, and a Reticon photodiode array detector. These are described in detail below. A schematic of the VUV spectrograph is Figure 4-3, and a scale drawing of the spectrograph and its view of

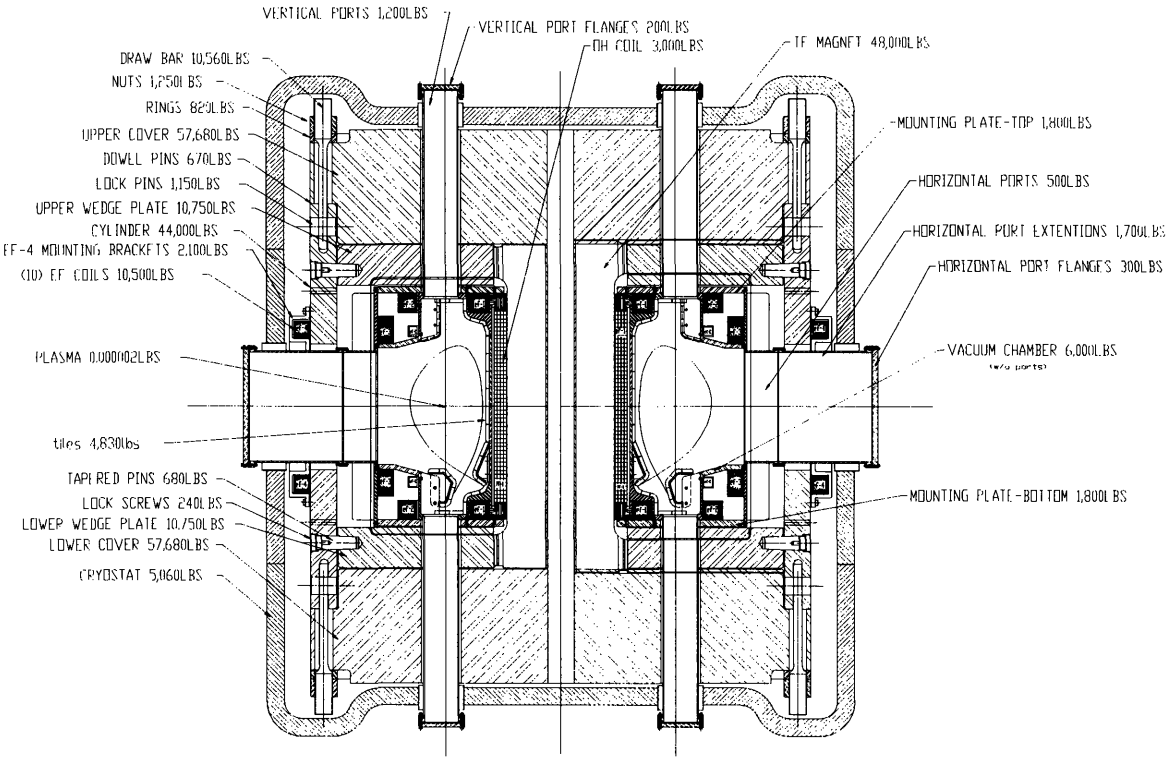

Figure 4-1: Cross-Section of the Alcator C-Mod Tokamak A more detailed view of the vacuum vessel cross-section is Figure 4-2.

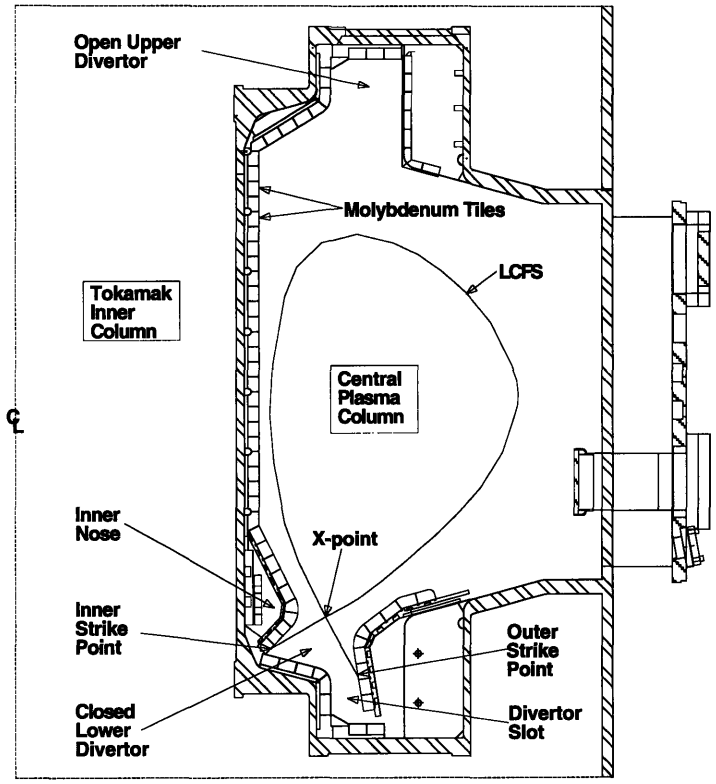

Figure 4-2: Vacuum Vessel Cross-Section The LCFS is the Last Closed magnetic Flux Surface, a useful reference surface.

the machine is Figure 4-4.

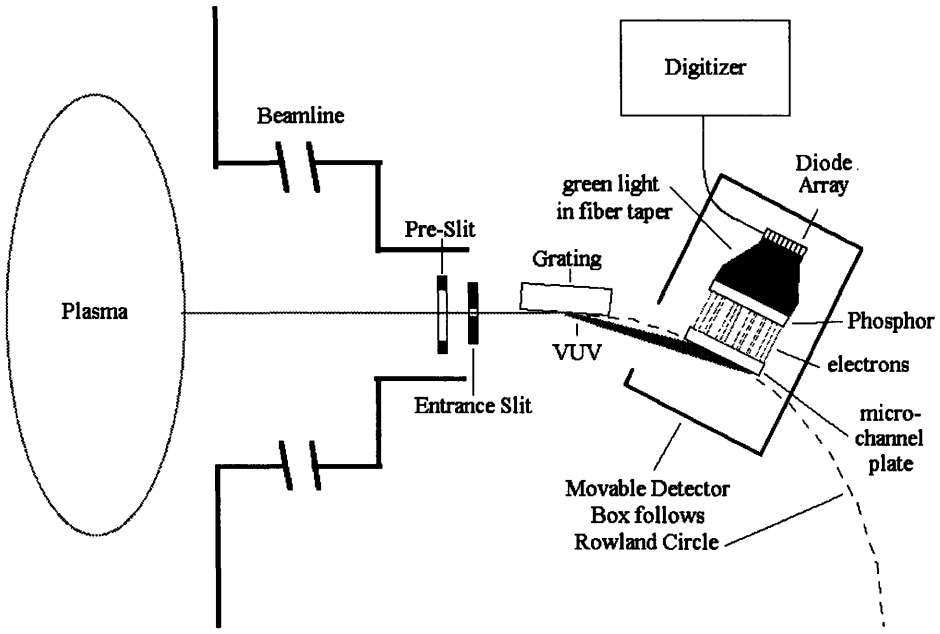

Figure 4-3: Schematic of the VUV Spectrograph This figure is not intended to show scale.

4.2.1 The grating

Radiation from the plasma travels down the VUV beamline and is incident on the entrance slit of the spectrometer, as shown in Figure 4-3. This entrance slit has adjustable width with range of 5 to 2000 μm, with typical widths being 50-150 μm. The radiation is diffracted by the grating according to the standard grating equation,

$$m\lambda = d(\sin\theta_i - \sin\theta_d), \tag{4.2}$$

where m is the order, d is the line spacing, θ_i is the incident angle, and θ_d is the diffraction angle. Both angles are measured from the grating normal.

The grating may be operated at several angles of incidence, from 82 to 88 degrees. The most oblique angle, 88 degrees, is used for these experiments, because it allows access to the lowest wavelengths. The grating used for the calibration has 300 ruled

lines per millimeter, allowing a spectral range from about 100 to 2200 Å in first order. The blaze angle is 2 degrees 4 minutes.

The grating has radius of curvature of 2.217 meters. The Rowland circle configuration puts the diffracted radiation in a horizontally (i.e. parallel to the grating grooves) focused image along a circle of diameter equal to the radius of curvature of the grating. A diameter of the Rowland circle is along the grating normal, and the circle is tangent to the grating face. The plane detector is moved precisely along an arc of this circle, as shown in Figure 4-3.

4.2.2 Microchannel Plate Image Intensifier

After diffracting off the grating, the radiation is detected by microchannel plate image intensifier mounted tangent to the Rowland circle. The photons strike a special photo-cathode coating on the front of the 40 mm diameter microchannel plate and unbind electrons with the appropriate work function. The plate coating (the photo-cathode) was cesium iodide, with a thickness of a few thousand angstroms.

The free electrons are swept down the angled channels by high voltage applied across the plate. The channels have diameter 10 microns and are spaced 12 microns apart. The free electrons are multiplied as they travel down the channel, with gain increasing with the voltage applied between the input and output faces of the plate. For plate voltage of 1000 V, the electron gain is on the order of 5×10^4. The multiplied electrons exiting the microchannel plate are accelerated across a 1 mm gap to strike a phosphor layer which luminesces visible photons.

The spatial distribution of the radiation, determined initially by the dispersion from the grating, is preserved by the channels. Therefore, the spatial distribution of the visible photons output by the phosphor is a function of the spectral distribution of the original VUV radiation.

The sensitivity of the microchannel plate image intensifier in converting VUV photons to visible photons is a function of the high voltage across the plate, the

voltage between plate and phosphor, and the quantum efficiency of the photocathode coating, which depends on the wavelength of the incident light.

4.2.3 Reticon photodiode array

The visible photons emitted by the phosphor are incident on a reticon photodiode array. The reticon has 1024 diodes, in a closely spaced linear array. The diodes are 2.5 mm high and are spaced 25 μm apart, center-to-center. The array controller outputs a voltage proportional to the time integrated photon flux incident on each diode, in sequence. The output is read by a digitizer. The integration time can be set between 4 and 4096 ms. The reticon pixel voltages thus are proportional to the VUV photon flux incident on the front of the intensifier. As a result of the dispersion off the grating, 1024 spectral bands are detected.

4.2.4 The view

Observing the radiation from a tokomak plasma is always complicated. The plasma can only be viewed through ports and windows, which fit snugly between toroidal coil windings. The large magnetic fields which confine the plasma can hinder the operation of the diagnostic. For this reason, detectors are often placed a few meters from the machine, where the magnetic fields fall to reasonable levels.

As shown in Figure 4-4, the VUV spectrograph views the plasma through a beamline extending from an eight inch wide port. A flexible bellows connects this 20 cm diameter beamline to the 20 cm flange at the front of the VUV spectrograph. This flange has a 10 cm beamline welded to the other face, which connects to the entrance slit of the grating box. The entire path of the beam, from plasma to detector, is kept under vacuum.

The spectrograph is mounted on a granite slab, which is supported by an aluminum stand. A jack at the rear of the stand (away from the plasma) tilts the stand about a pivot at the front (toward the plasma). The movement of the jack scans

the VUV instrument's view vertically across the plasma. These views are shown in Figure 4-4, and Figure 5-6. In tokamak studies, the vertical direction is mapped by the coordinate z, which is zero at the center of the cross-section.

When viewing the plasma along a major radial chord from the outside of the torus, changes in the horizontal direction move the view toroidally (see Figure 2-1). While there are interesting phenomenon which have toroidal variation or asymmetry, in general, there is toroidal symmetry in the emission, and variations are radial and poloidal. Some of these variations can be seen by scanning the view vertically. As discussed in Section 1.2, the VUV spectrograph data are used heavily in studies of radial transport which assume toroidal symmetry.

The vertical extent of the VUV spectrograph view is determined by the dimensions of a preslit (see Figure 4-3) which limits the cone of light which passes through the entrance slit and strikes the grating. In the calibrations, the preslit had a height of 0.146 cm, which corresponds to an angle of 0.0055 radians. This gives a spot height of $\sim$1.9 cm at the inner wall.

The horizontal (toroidal) extent of the view is determined by the height of the diode array, and the distance from the grating to the diode. The grating is positioned so that the light is diffracted vertically. The diode is aligned so that the long dimension of the individual diodes is horizontal. The toroidal extent of the view is therefore determined by the height of the individual diodes, which is 2.5 mm. The mapping of the diode view to the microchannel plate increases the effective area by a factor of 1.67.

The distance between the diode array and the grating must also be known, to determine the toroidal extent of the view. This distance varies with the observed central wavlength, as the detecting elements are moved along the Rowland circle. The range of distances used in the experiments corresponds to toroidal views of between 0.006 and 0.016 radians. The minimum angle is for observing longer wavelengths, and the maximum angle for shorter wavelengths. When mapped to the inner wall of

the vacuum vessel, these angles gives a spot width of 2-5 cm.

The brightness measured by the VUV spectrograph is the spatially averaged brightness along this view. The VUV spectrograph cannot resolve brightness variations which are spatially smaller than the extent of its view.

4.2.5 Previous Calibrations

The spectral sensitivity of the entire system is a complicated function, involving many factors. Some factors are known to degrade with time and use, such as the quantum efficiency of the microchannel plate CsI coating, and possibly the microchannel plate gain. The calibration must be checked regularly to remain reliable. Since the branching ratio method allows in situ measurements, frequent checks are both possible and convenient.

A great deal of work has been done in previous years [7] to calibrate the VUV spectrograph. The spectral sensitivity of the spectrograph has been calibrated before [7], when it was used with a 600 lines per mm grating. The calibration must be redone for each new grating and microchannel plate combination.

Previous calibrations have used a Manson soft x-ray source for the range from 20 to 114 Å, and a technique using doublet lines for wavelengths from 128 to 400 Å [7]. This thesis represents the first attempt at applying the branching ratio method for calibration of this instrument.

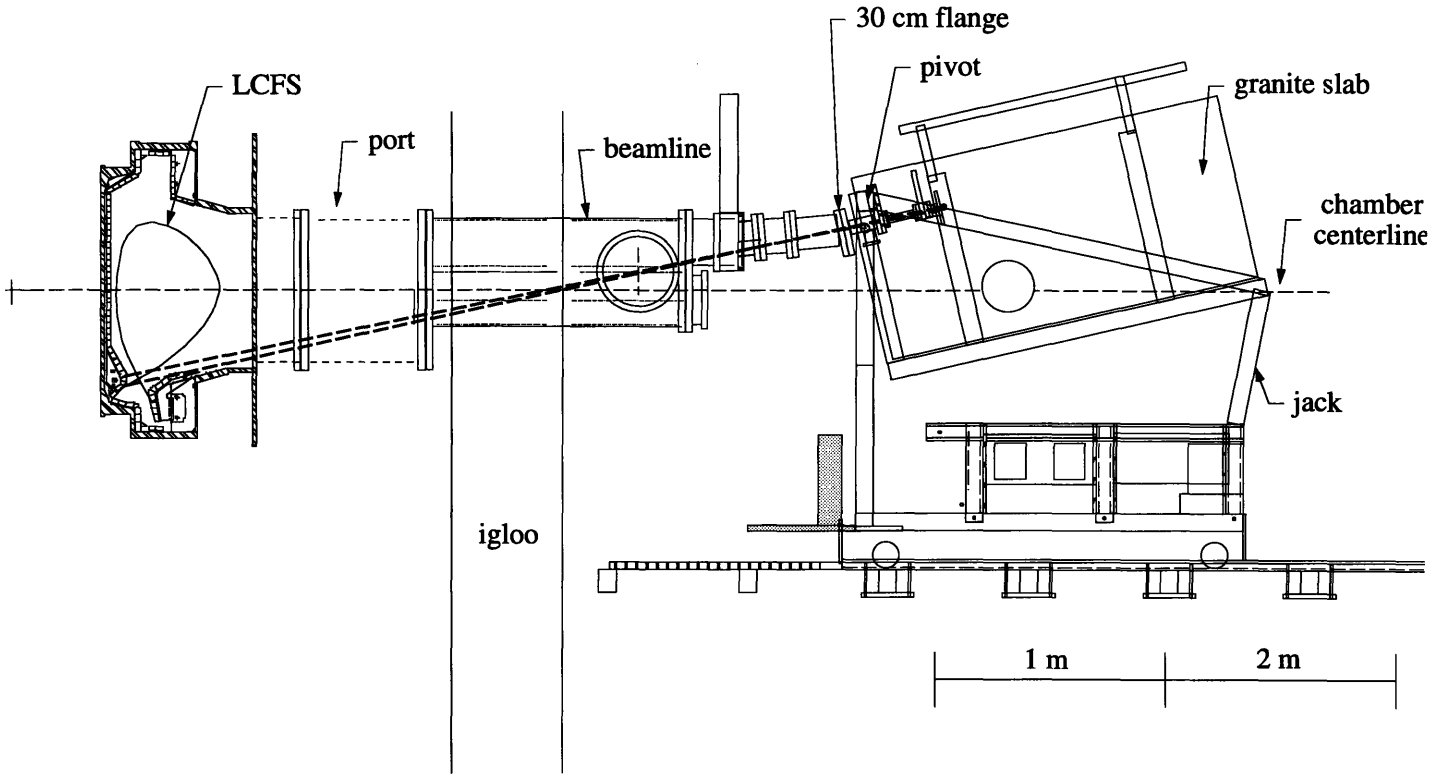

Figure 4-4: Scale drawing of the VUV Spectrograph's view of the vessel

Chapter 5

The Visible System

A system for viewing visible emission was specifically designed for calibration of the VUV spectrograph by the branching ratio method. The system has been designed to use two alternate visible detectors, either the CHROMEX spectrograph, or an interference filter/photomultiplier tube combination. The latter system was absolutely calibrated for four different interference filters. The CHROMEX has been absolutely calibrated from 3000 to 7000 Å.

5.1 The Apparatus

The VUV Visible Calibration System has three principal parts. The lens/fiber system provides the view of the plasma. The brightness of a chosen line is determined by either a lens/filter/fiber/photosensor or lens/fiber/CHROMEX spectrograph combination. A schematic of the system is Figure 5-2.

5.1.1 The Lens/Fiber System

The branching ratio calibration is done by comparing the brightnesses of the paired lines. The measured brightnesses are line integrated along the view and averaged over the solid angle of the view and the area of the detector. The brightness has units

power/steradian/area. The ratio of the brightnesses will equal the ratio calculated in equation (3.5), as long as the views are the same.

For a valid calibration, the two views need not be identical in toroidal extent, since the emission is toroidally symmetric to a high degree. However, it is critical that the plasma regions viewed by the two instruments do not have significantly different emissivity. Obviously, the intensities in two different regions of plasma are not necessarily linked by the branching ratio.

As discussed in Chapter 4, the VUV spectrograph averages over a region which extends approximately 2-5 cm in the horizontal (toroidal) direction, and 1.9 cm in the vertical, at the inner wall. The visible view was designed so that the maximum distance between the two beam paths was smaller than the extent of the VUV view.

For the visible view, a 2.54 cm diameter hole was cut in the face of the 20 cm flange (see Figure 4-4) at the front of the VUV spectrograph. A UV grade sapphire window was welded into the 2.54 cm hole. The shortest line measured for this thesis was 4686 Å, but future work may involve wavelengths down to 3000 Å. UV grade sapphire has good transmission (greater than 80%) down to around 2500 Å. *Since the 20 cm flange is attached to the VUV stand, the visible view is scanned with the VUV view as the jack is extended.*

The center of the 2.54 cm hole is offset 5.7 cm horizontally and 1.7 cm vertically from the center of the VUV beamline. When the views are aligned on the inner wall, there is a maximum distance between the beam paths in the plasma of 2.5 mm in the vertical dimension and 8.4 mm toroidally, as shown in Figure 5-1. Since the views average over a vertical region of $\sim$1.4 and $\sim$1.9 cm respectively, and since the emission is thought to be approximately uniform over this dimension, this "misalignment" is sufficiently small for reliable use of the branching ratio method.

A shelf bolted directly to the 20 cm flange face supports a lens and fiber which view the plasma through the sapphire window. The lens has nominal focal length of 50 mm, selected to give a spot diameter of 1.3 cm at the inner wall. The lens is an

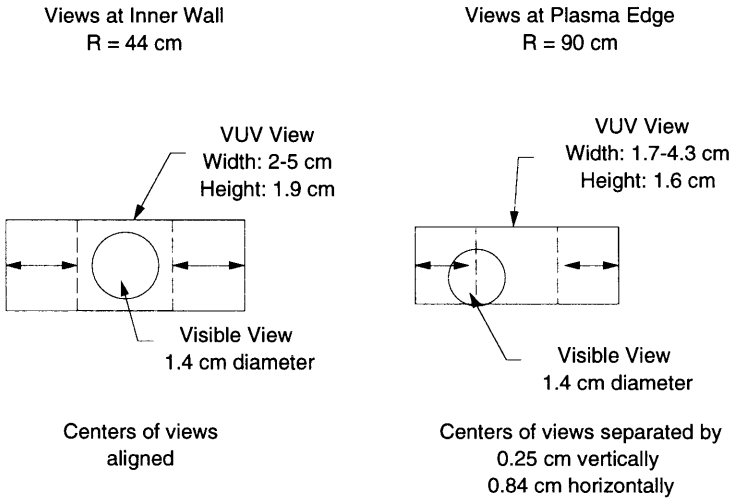

Figure 5-1: Comparison of Views of VUV Spectrograph and Visible System

achromat, to ensure that light at different wavelengths will have the same view of the plasma.

Achromats compensate for chromatic aberrations. The focal length of a lens is a function of the index of refraction, n, which in turn varies with the wavelength of the incident light, as given by the lens equation,

$$\frac{1}{f} = (n-1)\left(\frac{1}{R_1} - \frac{1}{R_2}\right), \tag{5.1}$$

where R_1 and R_2 are the radii of curvature for the two surfaces of the lens. In general for optical glasses, the index decreases with increasing wavlength. Therefore, for a single thin lens, the blue light is focused closest to the lens. When the image plane is at the focal plane of blue light, continuum light is imaged into a circular spectrum, with blue at the center, and red at the extremity. Clearly, with a single simple lens, light from different parts of the visible spectrum will have different views of the plasma. For the calibration, it is important that all measured lines have the same view of the plasma.

It is possible to construct a lens which has the same focal length for two different

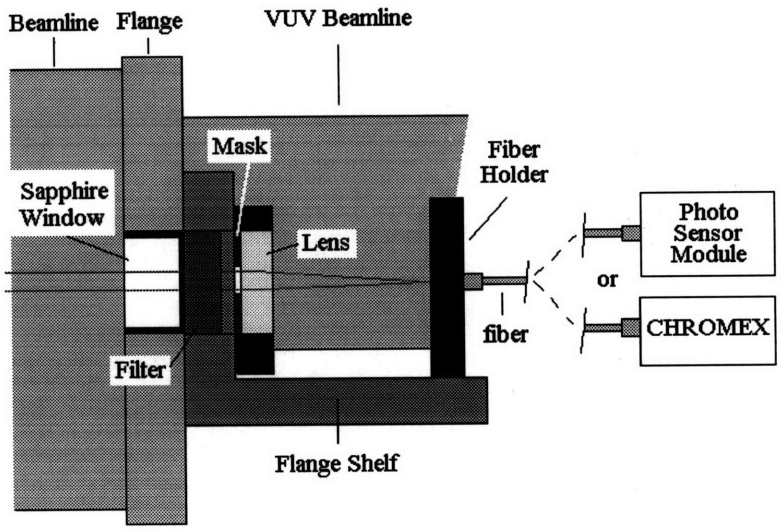

Figure 5-2: Visible System The face of the fiber is in the focal plane of the lens. The brightness in the fiber can either be measured by the photosensor module or the CHROMEX. This drawing is not intended to show scale.

wavelengths by combining two thin lenses, one convex and one concave. When two lenses are in contact, the combined focal length is given by

$$\frac{1}{f} = \frac{1}{f_1} + \frac{1}{f_2}. \tag{5.2}$$

For a convex lens, the quantity ρ, defined by

$$\rho \equiv \frac{1}{R_1} - \frac{1}{R_2}, \tag{5.3}$$

is negative, while for a concave lens, ρ is positive. Equating the focal length at two wavelengths, one red, one blue, gives

$$(n_{1B} - n_{1R})\rho_1 = -(n_{2B} - n_{2R})\rho_2. \tag{5.4}$$

This can be satisified by appropriate choices of the index of the two lenses, and as long as they are of opposite sign in ρ. The sign condition on ρ is satisfied by using

one convex and one concave lens. While the focal length can be made equal at two wavelengths, it is not equal at intermediate wavelengths, as shown in Figure 5-3. The lens used in this experiment had no noticeable chromatic aberration at intermediate wavelengths.

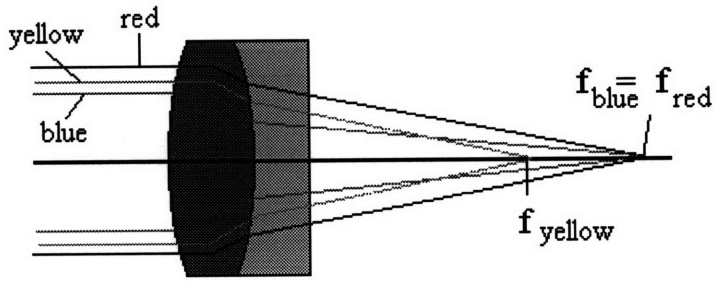

Figure 5-3: Achromat Doublet A convex and concave lens are cemented together to make a doublet with reduced chromatic aberration. The focal length is equal at one blue and one red wavelength. For intermediate wavelengths, the focus is closer to the lens.

The fiber is a 5.0 m long quartz fiber with a core diameter of 200 μm. It has excellent transmission across the wavelength region used in this calibration. Any loss within the fiber is negligible in comparison to reflection losses at the faces. The fiber is held by an adjustable fiber mount. The mount has two micrometers which move the fiber horizontally and vertically within a circle with diameter of 1.5 mm. This allows fine-tuning of the view, for alignment with the view of the VUV spectrograph. The face of the fiber is held in the focal plane of the lens. This positioning is very sensitive, and is performed by backlighting the fiber and adjusting the distance between the fiber and lens until the spot projected through the lens is focused at the desired distance.

To prevent coma, the 2.54 cm diameter lens is masked with an aperture of diameter 0.95 cm. Though this reduces the photon flux incident on the fiber, the mask was deemed necessary when coma caused significant image distortion in initial testing, which is discussed in Section 5.2.1.

5.1.2 Filter/Photosensor system

The Visible System was designed to be flexible, and the fiber can be output to any spectrometer within 5 m of the mount. For this thesis, a filter/PMT system and the CHROMEX spectrometer were used to measure the plasma radiation. The filters are 2.54 cm diameter interference filters. The filter holder fits on the flange shelf between the window and lens. The filters have peak transmission around 50%, and bandpasses of 20-26 Å. Four filters were used, with central wavlengths selected for viewing the lines given in Table 3.1.

In this configuration, the fiber is attached to a photosensor module manufactured by Hamamatsu. The photosensor outputs a voltage which is proportional to the intensity of the light carried by the fiber. The filters ensure that the light detected by the photosensor is from the appropriate line. The photosensor module houses a sensitive photomultiplier tube. The gain of the PMT is controlled by a voltage input, and is fully adjustable across four orders of magnitude. The photosensor has a sensitivity of up to 40 V/nW at the wavelenths of interest. The output voltage of the photosensor has range of +0-15 V, with a typical dark voltage of around 5 mV.

5.1.3 CHROMEX multi-view visible spectrometer

The CHROMEX spectrometer was used as an alternate detector of the emission within the view, and to measure the transmission function of the filters. The CHROMEX is designed for use with multiple, simultaneous views. Up to 14 fibers are imaged vertically along the entrance slit and dispersed by a grating in the horizontal direction. The dispersed light is imaged on a two-dimensional CCD detector. The CCD has 1242 spectral pixels. The light from an individual fiber is imaged on a band many pixels high. For a given fiber view, the output spectrum is averaged over the vertical band corresponding to that fiber.

For this calibration, only one fiber view was used, with either a 1200 or 1800 lines per mm grating.

5.2 Calibration

The Visible System was absolutely calibrated with an absolutely calibrated source, supplied by Labsphere, Inc. The view was aligned and focused by backlighting the fiber with a bright halogen bulb focused by a lens and mirror.

5.2.1 Testing the View

For alignment procedures, the fiber/lens system was backlit by a halogen bulb mounted in a mirror/lens configuration for maximum intensity at the focus. In early testing, it was found that coma was causing significant image degradation.

Coma is a primary lens aberration associated with object points which lie off the optical axis. In paraxial lens derivations, $\sin\phi$ is replaced by ϕ, where ϕ is the angle between the ray in the lens and the optical axis. Clearly, this is only valid for a narrow region around the axis. Primary aberrations are those which result from using this first order approximation for $\sin\phi$, and include spherical aberration, astigmatism, field curvature, and distortion.

The effect of coma is that meridional rays passing through the lens in different radial positions focus at different locations on the image plane. For lenses with negative coma, such as a planar-convex lens, the rays which pass through the lens further from the axis focus closer to the axis at the image plane, as shown in Figure 5-4. For positive coma, the more extreme rays focus further from the axis, as show in in Figure 5-5. Coma can be negated by placing an aperture in front of the lens [12]. The aperture prevents the large ϕ rays from passing.

When backlighting the Visible System, the beam spot has negative coma. In the experimental configuration, positive coma degrades the image of the plasma which is focused on the face of the fiber.

An adjustable aperture was placed in front of the lens, and contracted until the coma was sufficiently reduced. The diameter of the aperture was then measured, and found to be 0.95 cm. A 0.95 cm diameter mask was cut and mounted in the lens

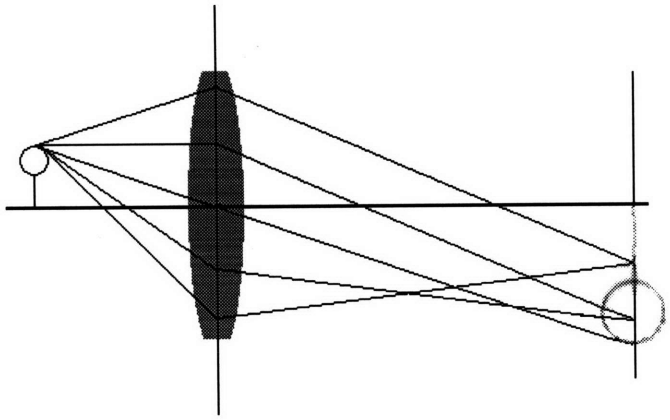

Figure 5-4: Negative Coma Planar-convex lenses have negative coma. Rays which pass through the lens further from the optical axis are focused closer to the axis at the image plane.

holder.

The masked lens produces a well focused spot. The spot diameter was measured to be 1.6 cm at a distance of 3.2 m, from image plane to lens. This is roughly equal to the diameter of 1.3 cm which is calculated using the simple lens equation and the nominal focal length. It was also found that movement of the micrometers across their entire 1.5 mm range results in movement of the spot within a circle of approximately 18 cm diameter. This range gives plenty of adjustment for alignment with the VUV view.

5.2.2 In-vessel Alignment

After the Visible System was mounted on the VUV stand, it was again backlit so that the spot could be observed on the vessel inner wall. The spot diameter was again measured, and found to be $\sim$1.4 cm. The spot was aligned with the VUV view at the jack position where the VUV view is known most accurately. Figure 5-6 shows the central chord of the view of the VUV spectrograph and the aligned Visible System in the vacuum vessel for several jack positions.

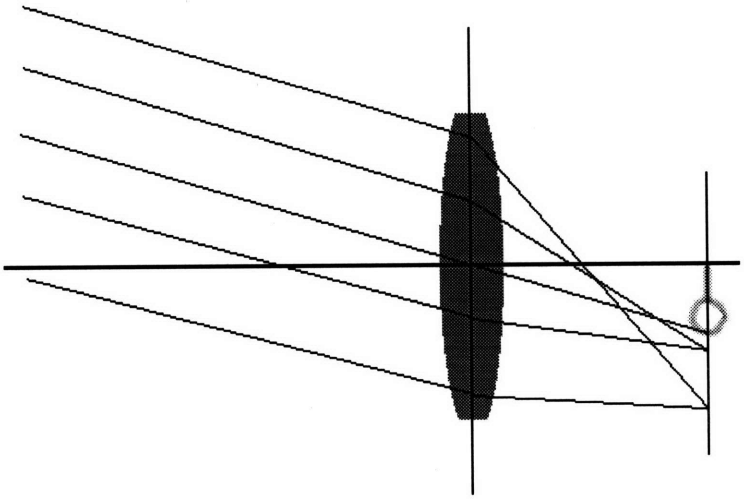

Figure 5-5: Positive coma Using a convex-planar lens to image a distant object results in positive coma. The rays which pass through the lens further from the optical axis focus further from the axis at the image plane.

The position of the spot on the inner wall was measured as the jack scanned the view vertically. From these measurements, the relationship between jack position and spot position was determined. It was found that the relationship derived from previous experiments was inaccurate.

The jack rotates the spectrograph about a pivot near the front of the stand. Given the geometry in Figure 5-7, the pivot angle, θ_{piv} is

$$\theta_{piv} = \text{acos}\left[\frac{a^2 + b^2 - d^2}{2ab}\right]. \tag{5.5}$$

The angles θ_1 and θ_2 are fixed angles, and therefore, their difference, defined θ',

$$\theta' \equiv \theta_2 - \theta_1 \tag{5.6}$$

is also constant. The angle of the view relative to the horizontal, θ_{plas}, is related to

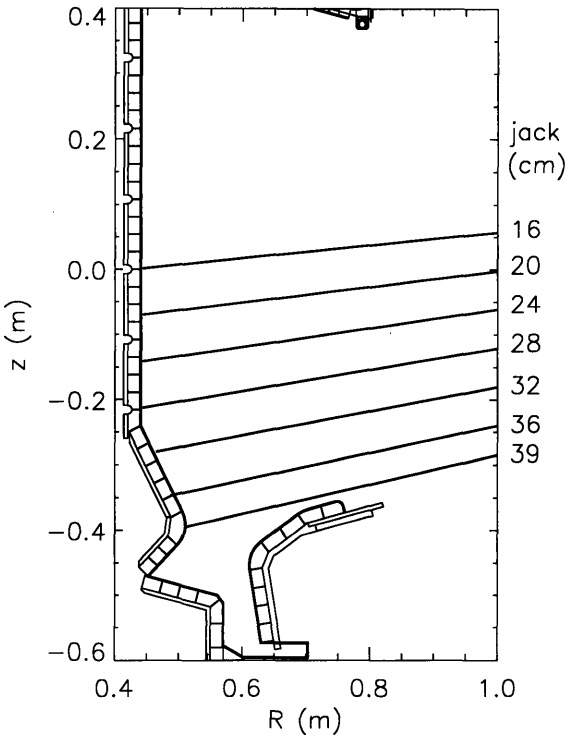

Figure 5-6: View of VUV Spectrograph for Several Jack Positions

θ_{piv} by

$$\theta_{plas} = \theta_{piv} + \theta'. \tag{5.7}$$

θ' is determined by using the θ_{plas} where the VUV spectrograph view is initially cut off by the outer divertor just beyond the lowest view position shown in Figure 5-6, and the calculated θ_{piv} for this jack position. Knowledge of θ_{plas} and the position of the pivot relative to the tokamak can then be used to calculate the z-coordinate of the strike point on the inner wall. After alignment of the Visible System view to the VUV view, the measured z_{strike} and the z_{strike} calculated from Equation (5.5) and

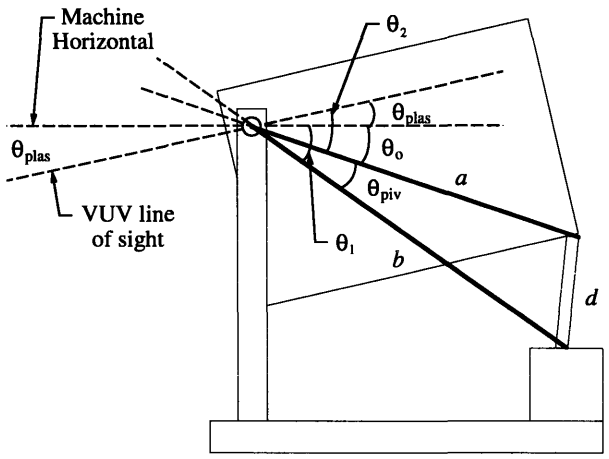

Figure 5-7: Dependence of Plasma Angle on Jack Extension
The figure is not to scale.

the jack extension are given in Table 5.1.

The quality of the alignment of the two views was checked by measurements during ECDC, as detailed in Section 6.4.5.

5.2.3 Sensitivity Calibration

The calibration source, referred to as the labsphere, after the manufacturer, provides continuum radiation from 3000 to 24000 Å. The intensity has been precisely absolutely calibrated by the manufacturer, and is given at twenty-six wavelengths with uncertainty of ~2.5%. The labsphere has a tungsten halogen lamp which illuminates the interior of a spherical cavity with highly diffuse reflective walls. Scattered light leaves the sphere through a circular two inch diameter opening in the cavity. The geometry of the labsphere is designed so that the light is uniform across the opening, and also uniform in angular distribution. In fact, the intensity falls off from its peak value at the center by 0.5% at the edge.

For the calibration, the Visible System, including the flange with sapphire window, was set up to view the labsphere. Since the calibration source has a known uniform

Jack Position cm	Plasma Angle radians	z_{strike} Calculated cm	z_{strike} Measured cm	Percent Discrepancy %
16.0	0.0996	+2.30	+2.40	+0.01
22.0	0.132	-10.6	-10.8	-0.15
27.8	0.162	-20.8	-20.1	+0.74
33.0	0.190	-29.8	-29.9	-0.05
35.6	0.203	-33.9	-34.0	-0.01
37.7	0.215	-37.3	-37.2	+0.01
38.1	0.217	-37.9	-37.7	+0.22
38.4	0.218	-38.4	-38.4	+0.01

Table 5.1: Comparison of Calculated View with Measured The discrepancy between the measured and calculated values is very small. The measured values have an estimated error of a few mm.

brightness over the opening, the extent of the view does not enter into the calibration, as long as the view of the instrument to be calibrated is entirely within the opening. In addition, the brightness measured by the detector should be independent of the distance between the labsphere and the Visible System. However, it was found that for distance less than about 30 cm, the brightness increases as the labsphere is brought closer. This effect is due to the interference filters, whose transmissions depend on the ray incident angle. Since the Visible System will be operating some 3 meters from the plasma, this near region effect is irrelevant.

The view was aligned so that the entire view of the fiber/lens system lay within the uniform source of the labsphere. It was confirmed that for distances greater than 30 cm, the signal measured by the Visible System was independent of the distance to the labsphere.

Photosensor Module

The filters used with the photosensor module have a bandpass of 20-26 Å. The output voltage of the photosensor is proportional to the total brightness of the source which

is passed by the filter, i.e.

$$V'_{out} = S \int B_{source}(\lambda) T_f(\lambda) d\lambda, \tag{5.8}$$

where S is the system sensitivity and the prime in V'_{out} denotes that the electronic noise background has been removed, i.e.

$$V'_{out} = V_{out} - V_{dark}. \tag{5.9}$$

For the branching ratio measurements, it was important that there were no significant contaminating lines or continuum radiation within the filter bandpass. In that case equation (5.8) becomes

$$V'_{out} = S B_{source}(\lambda_{line}) T_f(\lambda_{line}), \tag{5.10}$$

where $T_f(\lambda_{line})$ is the transmission of the filter at the wavelength of the line.

When viewing the labsphere, the photosensor sees a continuum of emission across the bandpass of the filter. Then the output voltage is

$$V'_{cal} = S \int B_{lab}(\lambda) T_f(\lambda) d\lambda, \tag{5.11}$$

where B_{lab} is the labsphere brightness.

The goal of the calibration of the Visible System with photosensor module is to determine the factor G_v which gives the true brightness of the plasma (assuming no contamination from other lines or continuum) at the desired line when multiplied by the signal voltage output of the photosensor, i.e.

$$G_v(\lambda_{line}, V_{cont})\, V'_{out} = B_{plasma}(\lambda_{line}). \tag{5.12}$$

G_v depends on the wavelength of the line, which includes the filter characteristics,

and the control voltage, V_{cont}, which determines the photomultiplier tube gain. The assumption of no contamination was verified in the experiment.

Comparison of equations (5.10) and (5.12) show that G_v can be written in terms of S as

$$G_v = \frac{1}{S T_f(\lambda_{line})}. \tag{5.13}$$

Then from equation (5.11),

$$G_v = \frac{\int B_{lab}(\lambda)\hat{T}_f(\lambda)d\lambda}{V'_{cal}}, \tag{5.14}$$

where $\hat{T}_f$ is the transmission of the filter, normalized by the transmission at the wavelength of the line, i.e.

$$\hat{T}_f(\lambda) = \frac{T_f(\lambda)}{T_f(\lambda_{line})}. \tag{5.15}$$

To determine G_v, the filter transmission function T_f must be measured. The transmission function of all filters was measured with the CHROMEX spectrograph, using the same lens/fiber system, and the labsphere as the source.

The lens/fiber system was set up to view the labsphere, now used simply as a continuum source for illumination, with the filter to be tested in place. The CHROMEX output of counts per second N_{out} is determined by

$$N_{out}(\lambda)' = C(I(\lambda, w_{slit}) * T_f(\lambda)), \tag{5.16}$$

where C is a constant, $I(\lambda, w_{slit})$ is the impulse response of the CHROMEX, * denotes convolution, and $T(\lambda)$ is the transmission function of the filter.

If the CHROMEX impulse response, I were a true impulse, the convolution would perfectly reproduce the transmission function T_f of the filter. The actual finite width impulse response results in broadening of the transmission function. For the best

reproduction of T_f, it is important that the impulse response of the CHROMEX be narrow in comparison to the bandpass of the filter. The CHROMEX impulse response is narrowest for small entrance slit widths. Therefore, the smallest slit widths which resulted in adequate signal were used.

A slit width, w_{slit}, of 20 μm was used for the bright H_α line. For the others, a slit width of 200 microns was needed for significant counts.

The impulse response $I(\lambda)$ was measured by using a hydrogen or helium lamp to supply the line of interest. The identical slit width, integration times, and grating were used as for the filter function measurements. The width of the impulse response depends on the slit width. The response at slit widths of 20 and 200 microns shown in Figures 5-8 and 5-9.

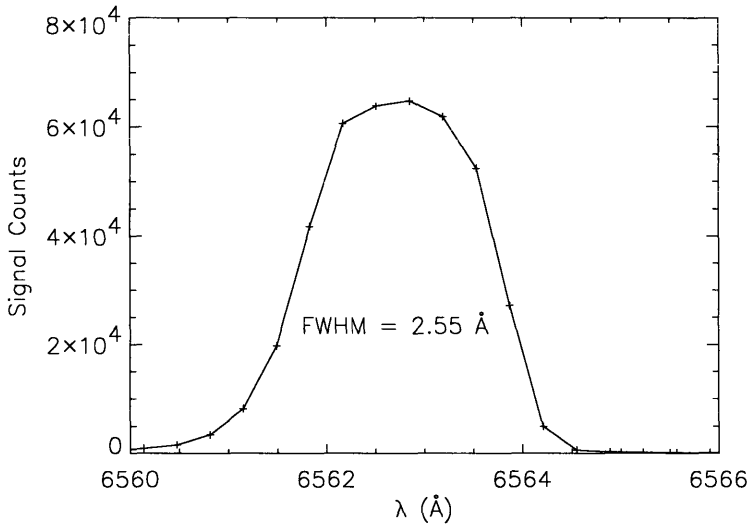

Figure 5-8: Impulse response of CHROMEX with slit width of 20 μ A CHROMEX input fiber was coupled to the output fiber of the Visible System, which was viewing a hydrogen lamp. The lamp provides H_α radiation at 6563 Å.

The results of the absolute measurements and the CHROMEX filter calibration must be combined to find G_v. A deconvolution was performed to find the filter function, as $I(\lambda)$ and $I(\lambda) * T_f(\lambda)$ are the known quantities in equation (5.16).

A good fit to $I(\lambda) * T_f(\lambda)$ was attained using a gaussian form for T_f. Normalized

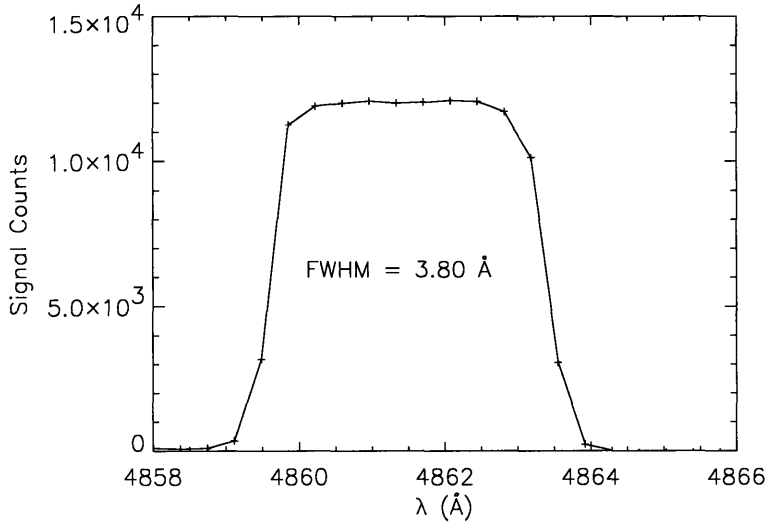

Figure 5-9: Impulse response of CHROMEX with slit width of 200 μ The CHROMEX viwed a hydrogen lamp through the Visible System. The observed line is H_β at 4861 Å.

$I(\lambda) * T_f(\lambda)$ for the D_β filter is shown in Figure 5-10, along with the fit generated by convolving a gaussian with $I(\lambda)$ given in Figure 5-9. It was found that the convolution with the impulse response does not appreciably broaden the transmission function, since the CHROMEX impulse response is so narrow in comparison to the filter bandbass. Taking the shape of $I(\lambda) * T_f(\lambda)$ as the shape of T_f results in an error of less than half a percent in the integral $\int T_f(\lambda) B(\lambda) d\lambda$.

Once the filter function is determined, G_v can be calculated from equation (5.14). The values for G_v found in this calibration are given in Table 5.2 and Figure 5-11. The only value used in the calibration which was not directly measured is the labsphere brightness, which was precisely calibrated by the manufacturer, and is the absolute standard for both the visible and VUV calibrations.

The values of G_v in Table 5.2 are for V_{cont} of 1 V, i.e., $G_v(V_{cont} = 1V)$. To find the dependence on V_{cont}, G_v must be divided by the gain of the photosensor module,

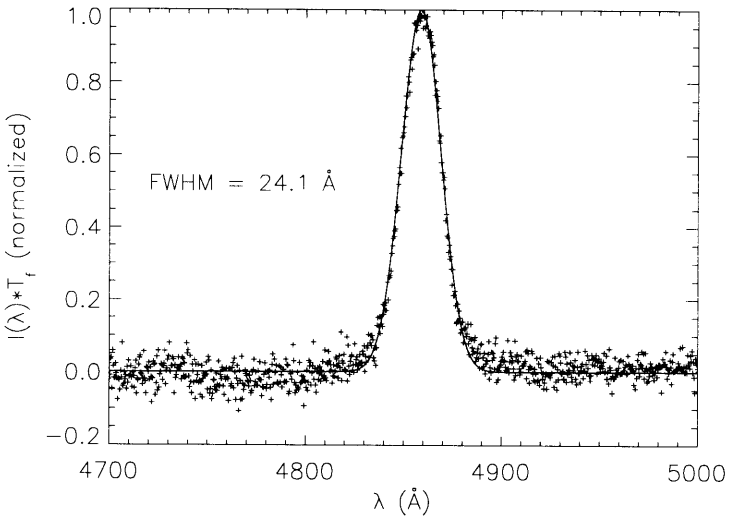

Figure 5-10: Normalized $I(\lambda) * T_f(\lambda)$ measured and calculated The symbols show the analyzed CHROMEX data. The line is the convolution of $I(\lambda)$ with a gaussian trial function for T_f.

g normalized to the value at 1V,

$$G_v(V_{cont}) = \frac{G_v(V_{cont} = 1V)g(V_{cont} = 1V)}{g(V_{cont})}. \tag{5.17}$$

The normalized photosensor gain is plotted versus control voltage in Figure 5-12.

Checking the absolute calibration

The values of G_v can be checked by estimating the sensitivity expected given the characteristics of the consituents of the system. The "typical" transmission of the window and the "typical" sensitivity of the photosensor are documented by the supplying vendors. G_v is then given by

$$G_v = (T_o\ \Omega\ A\ t_{wind}(\lambda_{line}) s_{pmt}(\lambda_{line}) T_f(\lambda_{line}))^{-1}, \tag{5.18}$$

λ_{line} Å	G_v Estimated W/st/m^2/V	G_v Measured W/st/m^2/V	Percent Discrepancy %
4686	0.0853	0.0967	-11.7
4861	0.0876	0.0886	-1.06
5016	0.0814	0.0845	-3.66
6563	0.1757	0.1621	+8.35

Table 5.2: Comparison of Estimated Sensitivity with Measured The values of G_v are for V_{cont} of 1V. The estimated and measured sensitivities agree to within $\sim$ 12%. These values are plotted in Figure 5-11.

where T_o is an overall, wavelength independent transmission factor for the system which includes reflections and other losses, Ω is the solid angle of the view, A is the area of the fiber face, t_{wind} is the transmission of the sapphire window, and s_{pmt} is the sensitivity of the photosensor, in units of volts/watt.

Ω and A are determined by the lens/fiber geometry. The transmission of the filter at the wavelength of the line $T_f(\lambda_{line})$ is found from the deconvolved filter function shape, normalized by the peak transmission quoted by the manufacturer. The fall off from the peak is around 5% for all the filters at the line of interest.

The factor T_o is primarily due to reflections at each surface. The achromatic lens has four surfaces, and the fiber has two. The reflection off the mirror is included in the window transmission. Therefore, T_o can be written as

$$T_o = (1 - R)^6, \tag{5.19}$$

where R is the reflection coefficient and is taken to be 5 %.

The estimated values for G_v are also given in Table 5.2, and Figure 5-11. The measured values are in excellent agreement, especially since the estimated values use the vendor-quoted, "typical" parameters for the components.

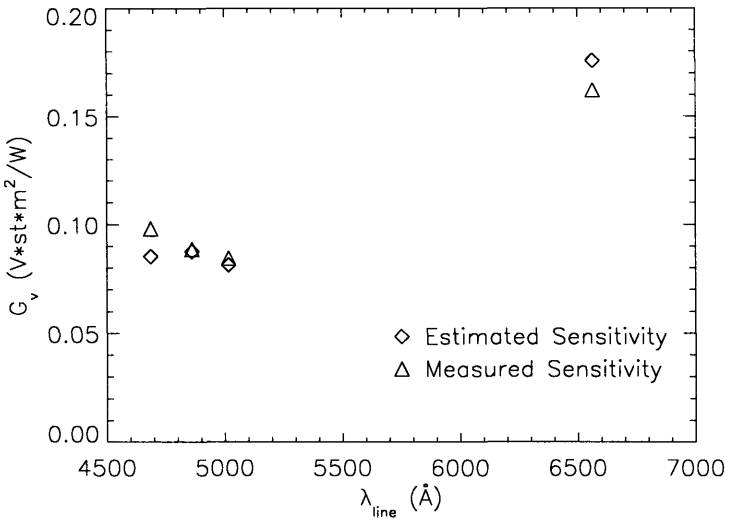

Figure 5-11: Measured and Calculated Visible System Sensitivity The calculated values are based on information supplied by vendors which are only intended to be approximate. Therefore, the above agreement, which is within 12%, is very good.

CHROMEX Sensitivity Calibration

The Visible System sensitivity was also calibrated with the CHROMEX as the detecting instrument. The Visible System fiber was connected to one of the 14 input fibers of the CHROMEX. The Visible System was then set up to view the labsphere. In contrast to the calibration of the photosensor module, no filters were used.

The desired factor, analogous to G_v, is R defined by

$$R(\lambda_{vis})N(line)' = B_{plasma}(\lambda_{vis}), \tag{5.20}$$

where $N(line)'$ is the total number of signal counts per second attributed to the desired line. With the labsphere continuum source, R is given by

$$R(\lambda) = \frac{B(\lambda)),\ \Delta\lambda}{N_{out}(\lambda)'} \tag{5.21}$$

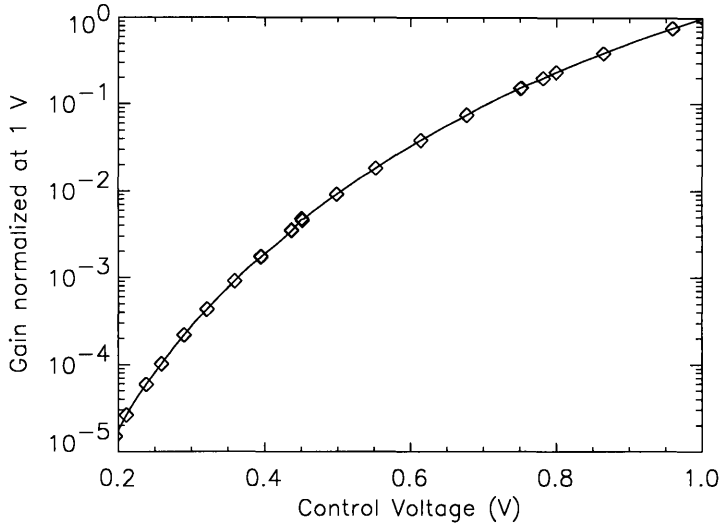

Figure 5-12: Photosensor Gain versus Control Voltage The gain is normalized to the value at 1V, the control voltage used in the calibration. The symbols represent measured values.

where $\Delta\lambda$ is the bandwidth of a single spectral bin.

This calibration was done in cooperation with D. A. Pappas. The spectral response was measured from 3000 - 7000 Å, for the 1200 lines per mm grating. The sensitivity for CHROMEX input fiber #1 (bin 1 in the CHROMEX software) is Figure 5-13.

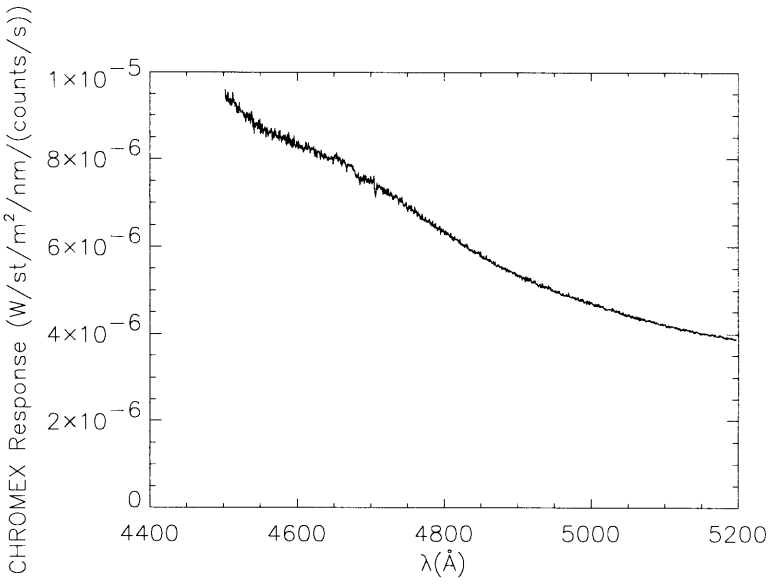

Figure 5-13: Spectral Response of CHROMEX Measurement was made with 1200 lines per mm grating.

Chapter 6

The calibration: results and analysis

Calibration measurements were made using the ECDC plasma and the fusion plasma as the sources. The lines listed in Table 3.1 were observed in deuterium and helium ECDC. In addition, D_α and D Lyman$_\beta$ were measured during a fusion discharge, for comparison.

6.1 Electron Cyclotron Discharge Cleaning

Electron cyclotron discharge cleaning is commonly used in tokomaks to reduce the impurity contamination of the plasma. Contamination is always a concern, and additional techniques, such as boronization of the vessel walls and baking (heating to greater than 130 degrees Celcius) the vacuum vessel are also used.

During discharge cleaning, a plasma is excited by microwaves inducing electron cyclotron resonance, and confined by toroidal fields, which are usually much smaller than those used for fusion plasmas. The plasma is typically hydrogen, deuterium or helium, with fill pressures on the order of 5×10^{-5} torr.

The electron cyclotron frequency is the frequency of an electron's gyration in a

uniform magnetic field. It is given by

$$\omega_{ce} = \frac{qB}{m_e}. \tag{6.1}$$

The toroidal magnetic field in a tokamak is approximated well by

$$B_{tor} = \frac{B_o R_o}{R}, \tag{6.2}$$

where B_o and R_o are the magnetic field and major radius at the center of the plasma. Since ω_{ce} is proportional to the magnetic field, it falls off as $1/R$.

The microwaves which are used for ECDC are at a fixed frequency of 2.44 GHz. Therefore, the microwaves are at the electron cyclotron frequency only at a particular major radius. In typical operation, the toroidal magnetic field is swept so that each region of the plasma will be at resonance for part of the sweep. The 2.44 GHz microwave frequency corresponds to a magnetic field of 0.087 T, a small fraction of the fields used to confine fusion plasmas.

Sweeping the field causes dramatic variation of the plasma brightness, as the resonance is moved. For the calibration, a source constant in time was desired, so the toroidal field was held nearly constant. The resulting plasma was very consistent in brightness over the course of many hours. However, there was some day to day variation (a factor of $\sim$2) even though all external parameters (microwave power, fill pressure, toroidal field) were nominally the same. The emission of the ECDC plasma had some spatial structure, as shown in Figure 6-12. Overall, ECDC was very well suited to use as a calibration source, as all of the proposed lines were measurable, and the data were consistent.

6.2 Preliminary Analysis

The goal of this thesis has been to find the factor which gives the true brightness of the plasma when multiplied by the total number of counts per second detected by the VUV spectrograph. This factor, called G_{VUV} then satisfies

$$G_{VUV}(\lambda_{VUV}, V_{phos}, V_{plat}, w_{slit}, w_{preslit}) N'_{VUV}(\lambda_{VUV}) = B_{plasma}(\lambda_{VUV}), \tag{6.3}$$

where N'_{VUV} is the number of signal counts per second on the VUV spectrograph from the desired line, V_{phos} is the phosphor voltage, V_{plat} is the voltage across the microchannel plate image intensifier, w_{slit}, is the width of the entrance list, and $w_{preslit}$ is the preslit width, which defines the vertical extent of the field of view. In Chapter 5 the similar factors, G_v for the filter/pmt system, and R for the CHROMEX were derived. They satisfy

$$G_v(\lambda_{vis}) V'_{out}(\lambda_{vis}) = B_{plasma}(\lambda_{vis}), \tag{6.4}$$

and

$$R(\lambda_{vis}) N'(line) = B_{plasma}(\lambda_{vis}). \tag{6.5}$$

In Chapter 3, it was shown that the brightnesses of a branching ratio pair have a known ratio (3.5). Then G_{VUV} can be calculated by either simultaneously measuring N'_{VUV} and V'_{out}, or N'_{VUV} and N', and using the equations below.

$$G_{VUV} = \frac{I_{VUV}}{I_{vis}} \frac{V'_{out}}{N'_{VUV}} G_v \tag{6.6}$$

$$G_{VUV} = \frac{I_{VUV}}{I_{vis}} \frac{N'_{out}}{N'_{VUV}} R \tag{6.7}$$

6.3 Calibration Procedures

The photosensor module has the advantages of being dedicated to the calibration and of being very simple. Therefore, the probability it will be available and operational is better than for the CHROMEX, which is also in demand for other measurements.

The CHROMEX is expected to give somewhat more accurate results, because

- Comparison of R and G_v show the CHROMEX to be more sensitive at long integration times
- It resolves the brightness into high resolution spectral bands, allowing for removal of background and contamination from neighboring lines.

Therefore, it is an important part of this calibration to determine how reliable the photosensor module results are, when compared to the CHROMEX data.

6.3.1 Deuterium ECDC

For deuterium ECDC, the chamber was filled with deuterium gas to a pressure of 5.0×10^{-5} torr. The Lyman series was measurable with the VUV spectrograph through Lyman$_\epsilon$, as shown in Figure 6-1. The visible lines D_α and D_β were dim, but detectable when the photosensor control voltage was set at the maximum value. Even at this highest gain, the output voltages were on the order of 100 mV.

For comparison, CHROMEX spectra were taken for both of the visible lines, D_α and D_β. It was important to determine the spectral contribution of the light which reaches the photosensor module, through the interference filters. The presence of other lines within the filter bandpass or significant continuum background will lead to errors when using the photosensor module. Therefore, measurements were also made by the CHROMEX with the various filters in place. A spectrum for D_β is Figure 6-2. For this spectra, the CHROMEX slit width was 200 μm, and the 1200 lines per mm grating was used. The filters effectively remove the background outside of the bandpass, but passes any continuum background within the bandpass.

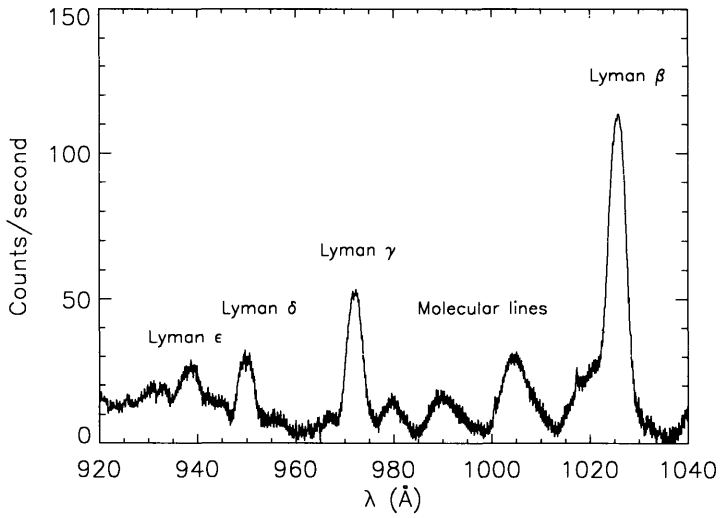

Figure 6-1: VUV spectrum of Deuterium Lyman Series The Lyman_{β} and Lyman_{γ} were used for the branching ratio calibration.

These CHROMEX spectra showed that the signal measured by the photosensor module comes overwhelmingly from the desired lines (>98%). The brightnesses calculated from the photosensor module results agreed with the CHROMEX brightnesses to within 5-7%. The discrepancy is more a result of calibration uncertainties than of contamination passed by the filter. This agreement shows that the photosensor module alone can be used for future calibration checks.

The determined values of G_{VUV} are presented in Table 6.2 and Figure 6-6. These

Parameter	Setting
Phosphor Voltage	-4600 V
Plate Voltage	-900 V
Repeller Voltage	-1000 V
Entrance Slit Width	200 μm
Right Pre-slit	12.02 mm
Left Pre-slit	10.39 mm
Pre-slit height	1.46 mm
Visible V_{cont}	1.0 V

Table 6.1: Settings for Calibration

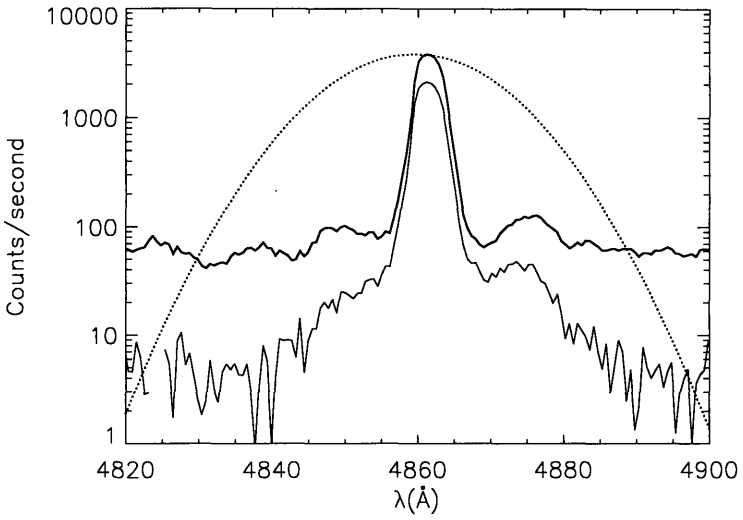

Figure 6-2: Comparison of filtered and unfiltered views The dotted line represents the transmission function of the filter, with arbitrary units. The thick line is the CHROMEX response with no filter. The thin line is the response with the 4861 Å filter. The filter blocks the background outside of the bandpass, but allows the neighboring line and background within the bandpass to contaminate the signal.

values of G_{VUV} are only valid at the VUV spectrograph gain voltages and slit widths used in the calibration, which are listed in Table 6.1. The dependence of the sensitivity of the VUV spectrograph on these factors is discussed in Section 6.3.5.

6.3.2 Helium ECDC

The lines observed in the helium discharge were in general less intense than those seen in the deuterium discharge. The intensity of the He II line at 4686 Å corresponded to only 3.1 mV of signal voltage on the photosensor module. At this low signal level, the fluctuations in the dark voltage make measurements with an accuracy of better than 20% impossible. Therefore, the calibration of the VUV spectrograph at the partner line He II Lyman$_\gamma$ (243 Å) was done with simultaneous measurements by the CHROMEX at 4686 Å. The results are given in Table 6.2 and Figure 6-6.

Complications arose with the He I 537/5016 Å line pair. The ratio between the CHROMEX counts per second and the VUV counts per second varied strongly with the pressure, as shown in Figure 6-5. The VUV line decreased in intensity with increasing pressure, like the observed lines in deuterium. The visible lines increased with increasing pressure, as in Figure 6-3.

It is believed that self-absorption of the VUV line is responsible for the variance of the ratio with the fill pressure. The effects of self-absorption are roughly given by

$$T = \mathrm{e}^{-knl}, \tag{6.8}$$

where T is the transmission, k is a constant which depends on the wavelength and oscillator strength of the line, the temperature, and the mass of the ion or atom, n is the number density of the absorbers, and l is the interaction length. From this equation it was roughly estimated that self-absorption results in a loss of ~25% of the He I 537 Å photons, at the lowest pressure which was used.

Self-absorption was negligible for the other lines because it is most important for transitions from the ground state of a neutral atom. Most of the interaction length was outside of the plasma, within the port and beamline. For deuterium, the gas was in a molecular state outside of the plasma, and therefore was not absorbing. The He II lines could not be absorbed by neutral helium atoms. And the visible He I line was not from the ground state, and therefore was also not absorbed by the cold helium atoms outside of the plasma.

A roughly estimated sensitivity was calculated at the He I line, assuming self-absorption loss of 25%. However, because the resulting sensitivity is so far outside the expected range, it is believed that self-absorption is significantly greater than the estimated value.

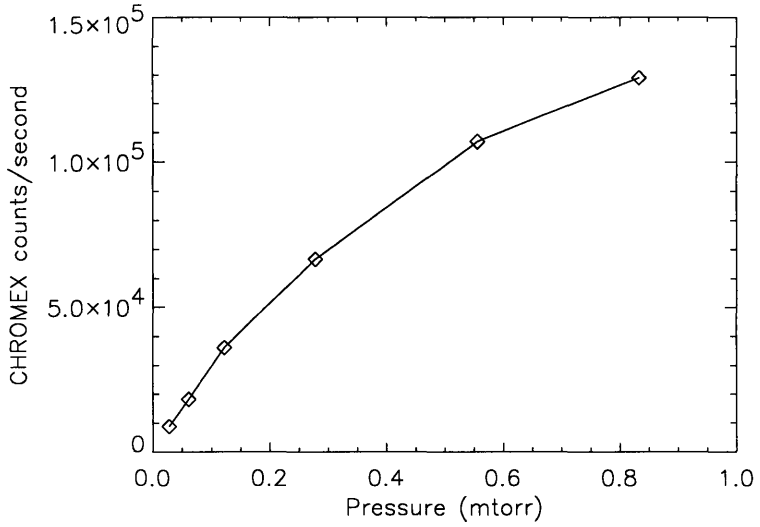

Figure 6-3: Visible Counts versus Fill Pressure

6.3.3 Fusion Plasma

Simultaneous measurements of D_α by the Visible System with photosensor module, and D Lyman$_\beta$ by the VUV spectrograph were made during fusion discharges. This shows the usefulness of the Visible System as a diagnostic with a scannable view, in addition to its role as a calibration tool. The time history of the line intensities evolved with an approximately constant ratio between the two lines, as shown in Figure 6-7. Note the very high time resolution of the Visible System ($>$ 5 kHz). The VUV sensitivity at D Lyman$_\beta$ found from the fusion plasma measurements was within 5% of that found during the very different conditions of ECDC plasma.

6.3.4 Discussion of the Errors

The minimum possible error in this calibration is determined by the uncertainty in the brightness of the labsphere. Allowing for drift of the brightness since the initial calibration, B_{lab} has estimated accuracy of $\sim$5%. Additional uncertainty is added by the various measurements in the calibrations.

The calibration factor associated with the photosensor module, G_v is based on

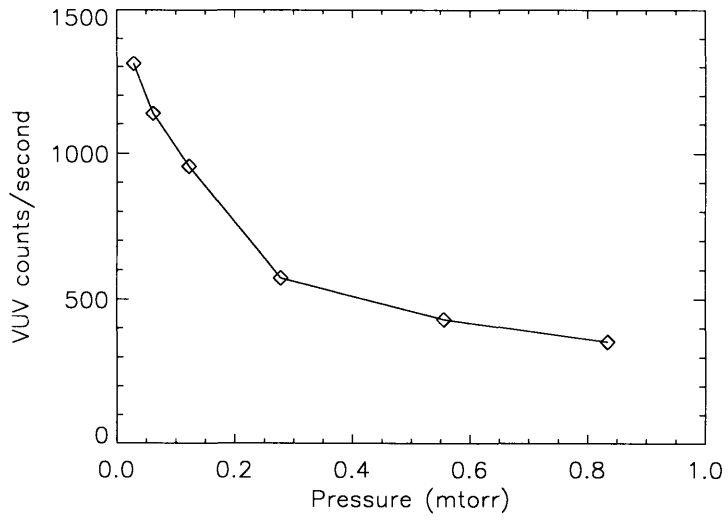

Figure 6-4: VUV Counts versus Fill Pressure

the measured filter response, the labsphere brightness, and the photosensor control voltage gain curve. Only the shape of the filter response was needed, allowing for a calibration accurate to within a few percent. The voltage gain curve had uncertainty of less than a percent. The propagated errors give an estimated uncertainty of ~10%.

The calibration factor for the CHROMEX, R, depends on the labsphere brightness and the bandwidth of a single spectral bin. This bandwidth is calculated very accurately by using reference lines to determine the wavelength corresponding to various bins. Therefore, the error associated with R is primarily due to uncertainty in B_{lab}.

The accuracy of calibration measurements of ECDC plasma depended on the signal level. For the photosensor module, measurements of D_α and D_β had accuracy of ~2-3%, but the very low signal He II 3s-4p line could not be measured with accuracy better than ~20%.

The VUV spectrograph measurements also had a range of signal levels. The D Lyman$_\beta$ and Lyman$_\gamma$ could be measured with accuracies of ~5%. The He II 1s-4p line was dim in comparison, and could only be measured with accuracy of ~10%. Measurements of the CHROMEX in all cases had accuracy of ~1% in the number of signal counts.

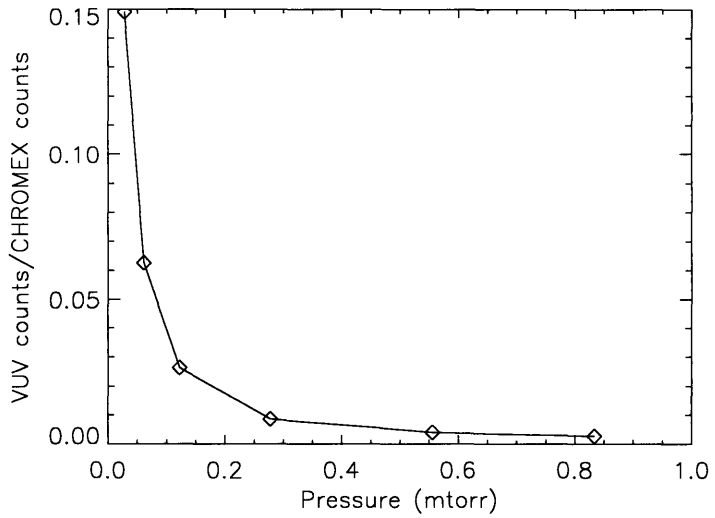

Figure 6-5: Ratio of VUV Counts to Visible Counts versus Fill Pressure The path integral of absorbers is given by the number density times the interaction length, in this case ~300 cm. The number density can be calculated from the pressure by multiplying by the factor 3.3×10^{13} parts/cm^{-3} mTorr, which is calculated for room temperature.

Because of the difficulties brought about by self-absorption of the He I line at 537 Å, the sensitivity estimated for this line is not included in the calibration, but is shown in Figure 6-6 for comparison.

The branching ratios for the three line pairs with no noticeable self-aborption are accurate to within ~0.1%, and therefore introduced negligible error.

The final calibration factor, G_{VUV} has an associated error of 12 - 17 % for the CHROMEX based measurements, and 15 - 35 % for measurements with the photosensor.

6.3.5 Additional Calibrations

The effects of the VUV spectrograph's control voltages and slit widths were also calibrated. The brightest VUV line in the ECDC plasma, D Lyman$_\alpha$ at 1215 Å, was

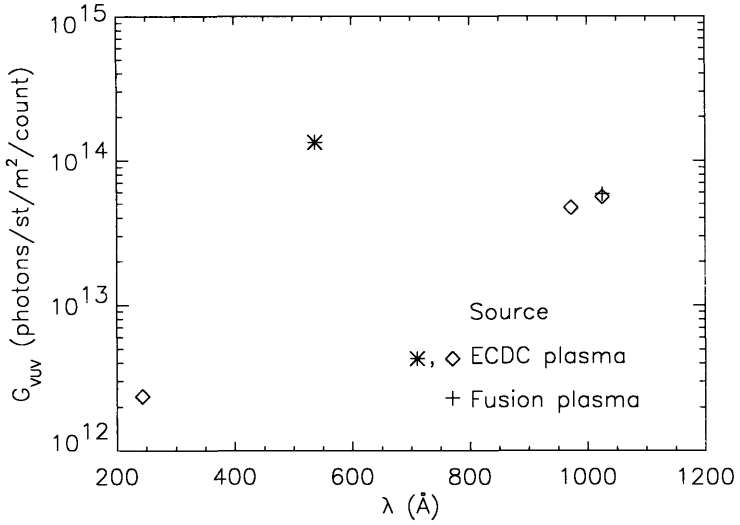

Figure 6-6: G_{VUV} versus wavelength Note that G_{VUV} at 537 Å is roughly estimated with self-absorption of 25%, and is only shown for comparison.

measured at various voltages and widths, using the Visible System measurement of D_α for normalization. The gains were normalized to those used in the G_{VUV} calibration, given in Table 6.1. The $G_{VUV}(\lambda)$ of the calibration is divided by these gain factors to find the $G_{VUV}(\lambda)$ for the set of voltages and slit widths, in the same manner as equation (5.20). Plots of the gain factors are Figures 6-8 - 6-10. The relative gain across the microchannel plate as detected by the diode array was measured the same way, and is given in Figure 6-11.

The VUV D Lyman$_\alpha$ and the visible D_α lines were also used to check the alignment of the two views. The two lines were measured at various jack positions. The signal versus jack position curves for the two lines should have the same shape, if the two views are aligned. It was found that the alignment was off by 0.5 cm in jack position, which corresponds to 1 cm on the inner wall. This was corrected by adjusting the VUV view relative to the visible view. The corrected signal versus jack position curves are Figure 6-12.

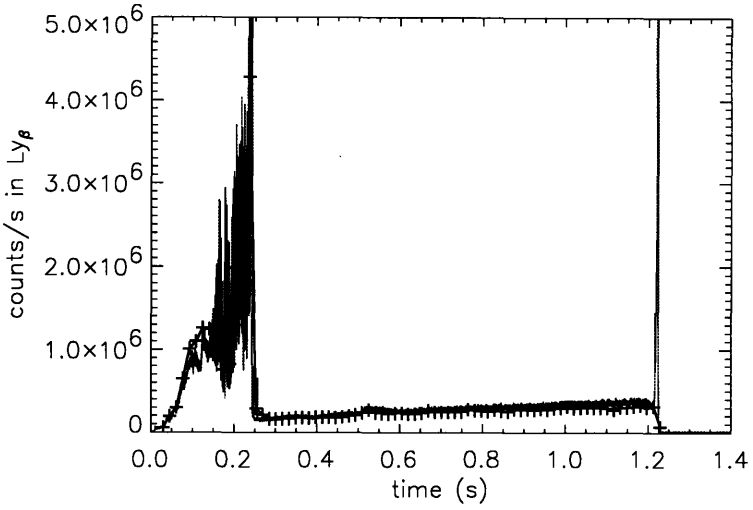

Figure 6-7: Comparison of Time Histories of D_α (solid gray line) and D Lyman$_\beta$ (symbols and solid black line) The D_α history is normalized for comparison with the D Lyman$_\beta$ history.

λ (Å)	G_{VUV} (photons/st/m^2/count)
243.03	$2.4\pm.4 \times 10^{12}$
972.27	$4.7\pm.6 \times 10^{13}$
1025.4	$5.6\pm.7 \times 10^{13}$

Table 6.2: Calibration Factors for VUV Spectrograph

6.4 Recommendations

The Visible System has not been used to its full potential. More line pairs can be used to fill out the spectral absolute calibration. Possible candidates includes lines from Li II, C III, C IV, and N IV, which are given in [6]. The branching ratio can also be employed with pairs of lines within the VUV, giving a relative calibration between two wavelengths in the VUV. Possible candidates are the He II line pairs 1s-3p (256 Å)/2s-3p (1640 Å), 1s-4p (243 Å)/2s-4p (1216 Å), and 2s-4p (1216 Å)/3s-4p (4686 Å). The latter two pairs were not possible in the ECDC plasmas described here because of contamination by D Lyman$_\alpha$ which is also at 1216 Å.

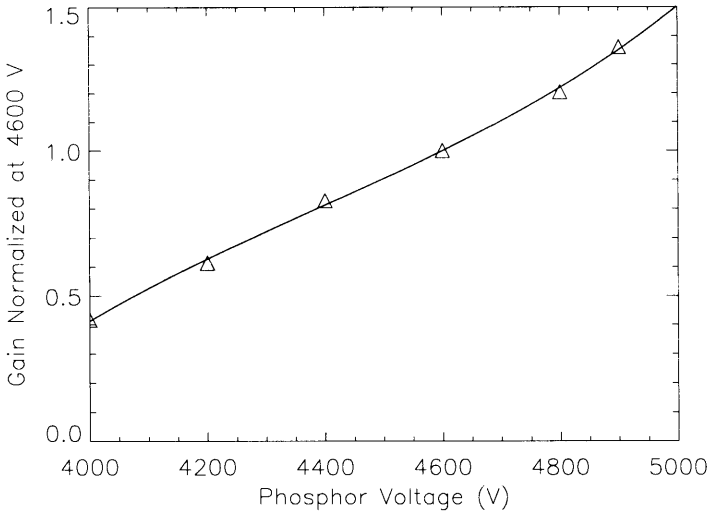

Figure 6-8: Gain versus Phosphor Voltage The symbols are the measured values, while the line is a third order polynomial fit.

The system is also useful for aligning or realigning the view of the VUV spectrograph. In the past, great care had to be taken in disassembly and reassembly to insure that the view was not altered. With the Visible System, the alignment can be checked by measuring the position of a backlit visible spot. The coincidence of the views can be measured by scanning the ECDC plasma.

The increased accuracy of the absolute calibration of the VUV data will make it more useful. It is consequently important that the accuracy of the calibration be maintained through regular checks, to keep a record of any changes in sensitivity.

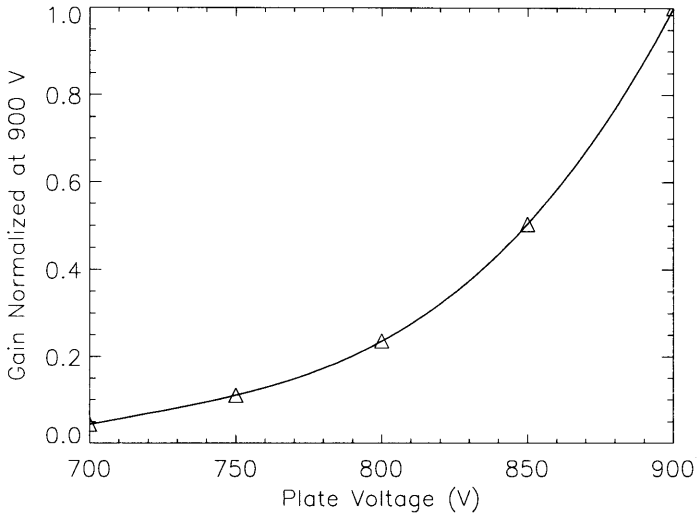

Figure 6-9: Gain versus Plate Voltage The plate voltage is the voltage across the microchannel plate image intensifier. The symbols are the measured values, while the line is a third order polynomial fit.

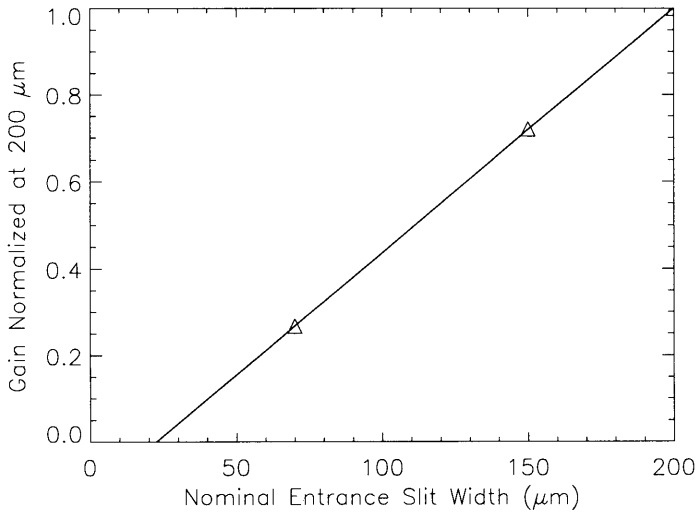

Figure 6-10: Gain versus Nominal Entrance Slit Width The symbols at 70, 150, and 200 μm are the measured values, while the line is a linear fit. Note that the slit is in fact closed at a nominal width of 22.6 μm.

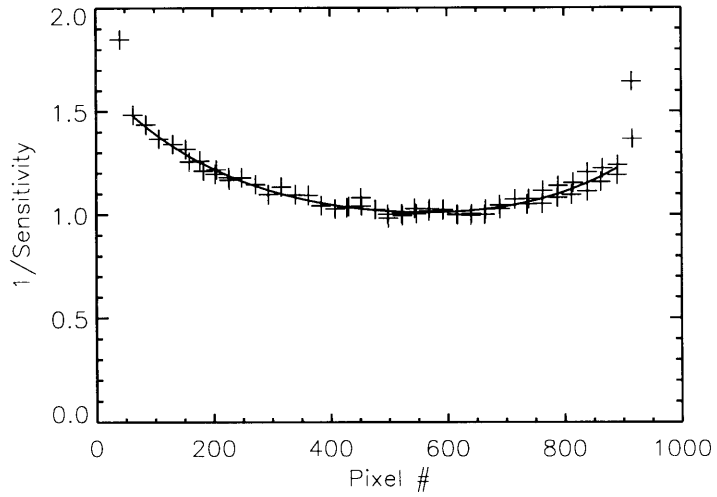

Figure 6-11: Gain versus Pixel Number

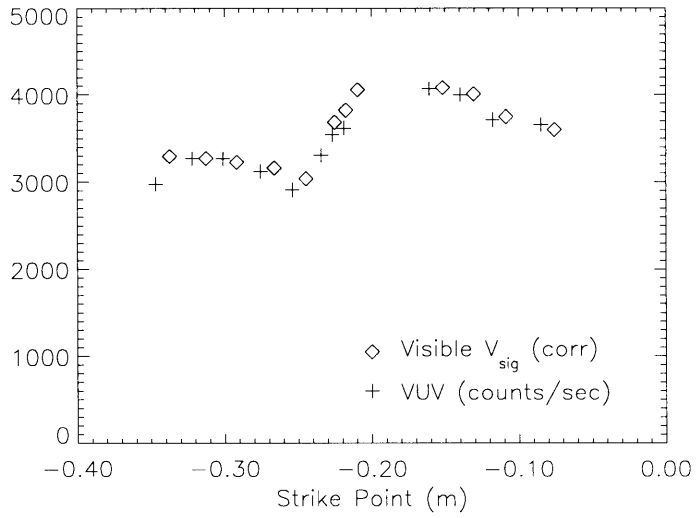

Figure 6-12: Signal versus Strike Point on Inner Wall The visible signal is shifted by .003 radians in plasma angle, which corresponds to 1 cm in the strike point, and normalized to give the best agreement with the VUV signal.

Chapter 7

Summary

The VUV spectrograph of Alcator C-Mod was absolutely calibrated at three wavelengths with the branching ratio method. This technique uses the known branching ratio between transitions which share the same upper state. Pairs are chosen with one line in the spectral range of the VUV spectrograph, and the other in the range of an absolutely calibrated visible instrument.

In addition to the absolute sensitivity, calibrations of the VUV detector gains, the relative sensitivity across the detector, and the slit width were performed.

For valid use of the branching ratio technique, the two instruments must view the same, or approximately the same source. In the tokamak, this means they must share the same line of sight, to view the same region of plasma. Consequently, a Visible System was designed and built with a lens/fiber combination which mounts directly on the scanning VUV spectrograph stand. Thus, the two views move together, as the stand pivots, and are physically separated by a negligible distance. The Visible System was calibrated using a precisely absolutely calibrated uniform source.

Electron cyclotron discharge cleaning (ECDC) and fusion plasmas were used as the calibration sources. Two line pairs of D I, (972/4860 Å), and (1025/6561 Å), and one line pair of He II, (243/4686 Å) were used successfully for branching ratio calibration measurements. A fourth pair, He I, (537/5016 Å) was found to be unsuitable because

of self-absorption of the 537 Å line at the pressures currently used for ECDC.

Accurate absolute calibration of the VUV spectrograph is essential for several ongoing studies on C-Mod. The VUV spectrograph data is used to "calibrate" a 1-D transport computer model which determines impurity density profiles. It is also used in the impurity screening experiments which study the degree to which the impurities in the divertor are screened from the core plasma.

The Visible System remains operational, for future checks of the calibration, additional calibration measurements, and also as the only scannable visible view of the C-Mod plasma.

Appendix A

Calibration Data

The photosensor gain curve of Figure 5-12 was created by the IDL procedure
user10:[ohkawa]hamavolt.pro

The CHROMEX sensitivity information given in Figure 5-13 is available as an IDL save file
mist$root:[graf]chrom.sav

The VUV spectrograph gain curves in Figures 6-8, 6-9, and 6-10 were created by

user10:[ohkawa]phoscal.pro	(Gain vs. Phosphor Voltage)
user10:[ohkawa]platcal.pro	(Gain vs. Plate Voltage)
user10:[ohkawa]slitcal.pro	(Gain vs. Plate Voltage)

The relative sensitivity across the plate in Figure 6-11 is also available as an IDL save file
mist$root:[graf]sens.sav

The V_{cont} of the photosensor module is set by the following IDL commands:
IDL> .r user10:[ohkawa]set_hana_hv

IDL> setup_mcpvis

IDL> mcpvis_volt

In mcpvis_volt, the user selects the voltage setting from a menu.

To import CHROMEX data into IDL,

- 'Save as' the WinSpec .spe file in the Generic (.gen) format.
- Use Rapid Filer to transfer the .gen file to a workstation.
- Read the file into IDL with user10:[ohkawa]read_frame12.pro, or latest version (see Dmitrios Pappas). The call is **read_frame12, 'filename', counts** where counts is the output variable. For wavelength calibration, see Dimitrios Pappas.

Bibliography

[1] G. M. McCracken, B. Lipschultz, et al. Impurity screening in ohmic and high confinement plasmas in the Alcator C-Mod tokamak. *Physics of Plasmas*, 1997.

[2] J. E. Rice, J. L. Terry, et al. X-ray and VUV observations of Mo^{23+} Mo^{33+} brightness profiles from Alcator C-Mod plasmas. *Journal of Physics B*, 29, 1996.

[3] F. P. Chen. *Introduction to Plasma Physics and Controlled Fusion.* Plenum Press, 1984.

[4] D. Halliday and R. Resnick. *Fundamentals of Physics.* Wiley and Sons, 1988.

[5] A. N. Zaidel and E. Shreider. *Vacuum Ultraviolet Spectroscopy.* Ann Arbor-Humphrey Science Publishers, 1970.

[6] J. Z. Klose and W. L. Wiese. Branching ratio technique for vacuum UV radiance calibrations: Extensions and a comprehensive data set. *J. Quant. Spectrosc. Radiat. Transfer*, 42, 1989.

[7] M. Graf. *Impurity injection experiments on the Alcator C-Mod tokamak.* Ph.D. Thesis, Massachussetts Institute of Technology, 1995.

[8] H. G. Kuhn. *Atomic Spectra.* Longmans Green, 1969.

[9] G. Herzberg. *Molecular Spectra and Molecular Structure.* Van Nostrand Reinhold, 1950.

[10] G. Herzberg. *Atomic Spectra and Atomic Structure.* Dover Publications, 1944.

[11] P. Stek. *Reflectometry Measurements on Alcator C-Mod.* Ph.D. Thesis, Massachussetts Institute of Technology, 1997.

[12] E. Hecht. *Optics.* Addison-Wesley Publishing Company, 1987.

[13] A. R. Striganov and N. S. Sventitskii. *Tables of Spectral Lines of Neutral and Ionized Atoms.* Plenum Press, 1968.

[14] J. Reader, C. H. Corliss, W. L. Wiese, and G. A. Martin. *Wavelengths and Transition Probabilities for Atoms and Atomic Ions.* U. S. Government, 1980.